

Multi-cancer molecular signatures and their interrelationships

Wei-Yi Cheng¹, Tai-Hsien Ou Yang¹, Hui Shen², Peter W. Laird², Dimitris Anastassiou¹ and the Cancer Genome Atlas Research Network

¹*Columbia Initiative in Systems Biology and Department of Electrical Engineering, Columbia University, New York, NY, USA*

²*USC Epigenome Center, Norris Comprehensive Cancer Center, Keck School of Medicine, University of Southern California, Los Angeles, CA, USA.*

Corresponding Author Dimitris Anastassiou, Columbia Initiative in Systems Biology and Department of Electrical Engineering, Columbia University, 1312S.W.Mudd Building, – Mail Code 4712, 500 West 120th Street, USA. Phone:+1212854-3113; E-mail: da8@columbia.edu

This is version 2. A previous version of the same article appears at <http://arxiv.org/pdf/1306.2584v1.pdf> dated June 11, 2013.

Please note: The pan-cancer molecular signatures disclosed in this article are the results of applying our data mining algorithm to the rich TCGA “pancan12” data sets from twelve different cancer types. These signatures have been identified as patterns, without any indication about their role or potential usefulness. We believe that each of them represents an important biomolecular event in cancer.

We invite the cancer research community to contact us and help us interpret each of these pan-cancer signatures, and to investigate them for potential applications in diagnostic, prognostic and therapeutic products applicable to multiple cancer types. There will be additional versions of this article and we expect that the final version will contain many co-authors.

Although cancer is known to be characterized by several unifying biological hallmarks, systems biology has had limited success in identifying molecular signatures present in all types of cancer. The current availability of rich data sets from many different cancer types provides an opportunity for thorough computational data mining in search of such common patterns. Here we report the identification of 18 “pan-cancer” molecular signatures resulting from analysis of data sets containing values from mRNA expression, microRNA expression, DNA methylation, and protein activity, from twelve different cancer types. The membership of many of these signatures points to particular biological mechanisms related to cancer progression, suggesting that they represent important attributes of cancer in need of being elucidated for potential applications in diagnostic, prognostic and therapeutic products applicable to multiple cancer types.

Cancer is known to be not just one disease, but many diseases, as evidenced by the diversity of its pathological manifestations. On the other hand, it has been appreciated that there exist some unifying capabilities, or “hallmarks,” characterizing all cancers, as proposed in two seminal papers^{1,2}. It is reasonable to hypothesize that such common biological traits would be represented by particular patterns detectable in data sets derived from cancer samples. However, systems biology has had limited success in finding such common patterns until recently. The current availability of integrated biomolecular data sets from twelve cancer types (“pancan12”) in The Cancer Genome Atlas (TCGA) provides an opportunity for thorough data mining, so that such common patterns can be computationally discovered and defined with high accuracy.

Our data mining approach³ uses an iterative algorithm to identify patterns that manifest themselves as distinct molecular signatures, called attractor metagenes, several of which were found in nearly identical form following separate analysis of data sets from multiple different cancer types. The algorithm is designed to converge to the core of gene coexpression patterns, without being influenced in any way by other constraints, such as classification of samples into subtypes. These signatures are manifested by the coordinate observed presence of many features (such as expression of genes or methylation of genomic sites), to varying degrees, in multiple cancer types. The three main molecular signatures that we previously found³ using data sets from three cancer types are associated with mitotic chromosomal instability (CIN), mesenchymal transition (MES) and a lymphocyte-specific immune recruitment (LYM). We hypothesized that these molecular signatures represent important biomolecular events of cancer, and therefore that they would be associated with phenotypes in multiple cancer types. Consistent with this hypothesis, a computational model using attractor metagenes as features recently won the Sage Bionetworks/DREAM Breast Cancer Prognosis Challenge^{4,5}.

Here we report our results of discovering “Pan-Cancer” molecular signatures applying the same computational methodology (**Methods**) on the TCGA pancan12 data sets. Based on parameter choices that would guarantee that such signatures are clearly present in the majority of the data sets and would involve a significant number of mutually associated genes.

RESULTS

Listing of 18 Pan-Cancer signatures

We identified 15 attractor molecular signatures, seven of which were present in mRNA expression data sets, three in DNA methylation data sets, three in microRNA expression data sets, and two in protein activity data sets. We found several additional genomically co-localized molecular signatures, mainly representing amplicons, and we report on three of them, for a total of 18 attractor signatures.

The signatures identified separately in individual cancer types available under Synapse ID syn1899444. The consensus ranked lists for each of these signatures are presented in **Table S1**, as well as under Synapse ID syn1899445. We also identified genomically co-localized molecular signatures, presented under synapse ID syn1899446. The first two such signatures (MHC Class II and GIMAP gene cluster) are strongly associated with the LYM metagene. The third signature contains the Pan-Cancer chr8q24.3 amplicon, which we had previously identified³ as the strongest amplicon attractor metagene.

We confirmed that the three main attractor metagenes (CIN, MES, LYM) that we previously identified³ are the most prominent ones (using a measure of signature strength defined in **Methods**) among all 18 signatures. In addition, we identified several new attractor metagenes resulting from this new thorough analysis, one of which (END) contains endothelial markers and is associated with angiogenesis.

A striking visualization consistent with the co-expression of these Pan-Cancer molecular signatures can be made in the form of scatter plots. For example, **Fig. 1** shows such color-coded scatter plots for the four main attractor metagenes CIN, MES, LYM, and END, in all twelve cancer types using the three top-ranked genes for each of these four signatures. In each scatter plot, samples represented by dots at the lower left (blue) side have low levels of the signature, while samples represented by dots at the upper right (red) side have high levels of the signature. **Fig. S1** shows the corresponding scatter plots for all 18 identified attractor molecular signatures demonstrating such coexpression in all cases. Scrutinizing each of these molecular signatures provides opportunities for discovery in cancer biology.

Table 1 provides a summary of the 18 signatures, including brief comments and a listing of their top-ranked members. In the following , we briefly describe each of them.

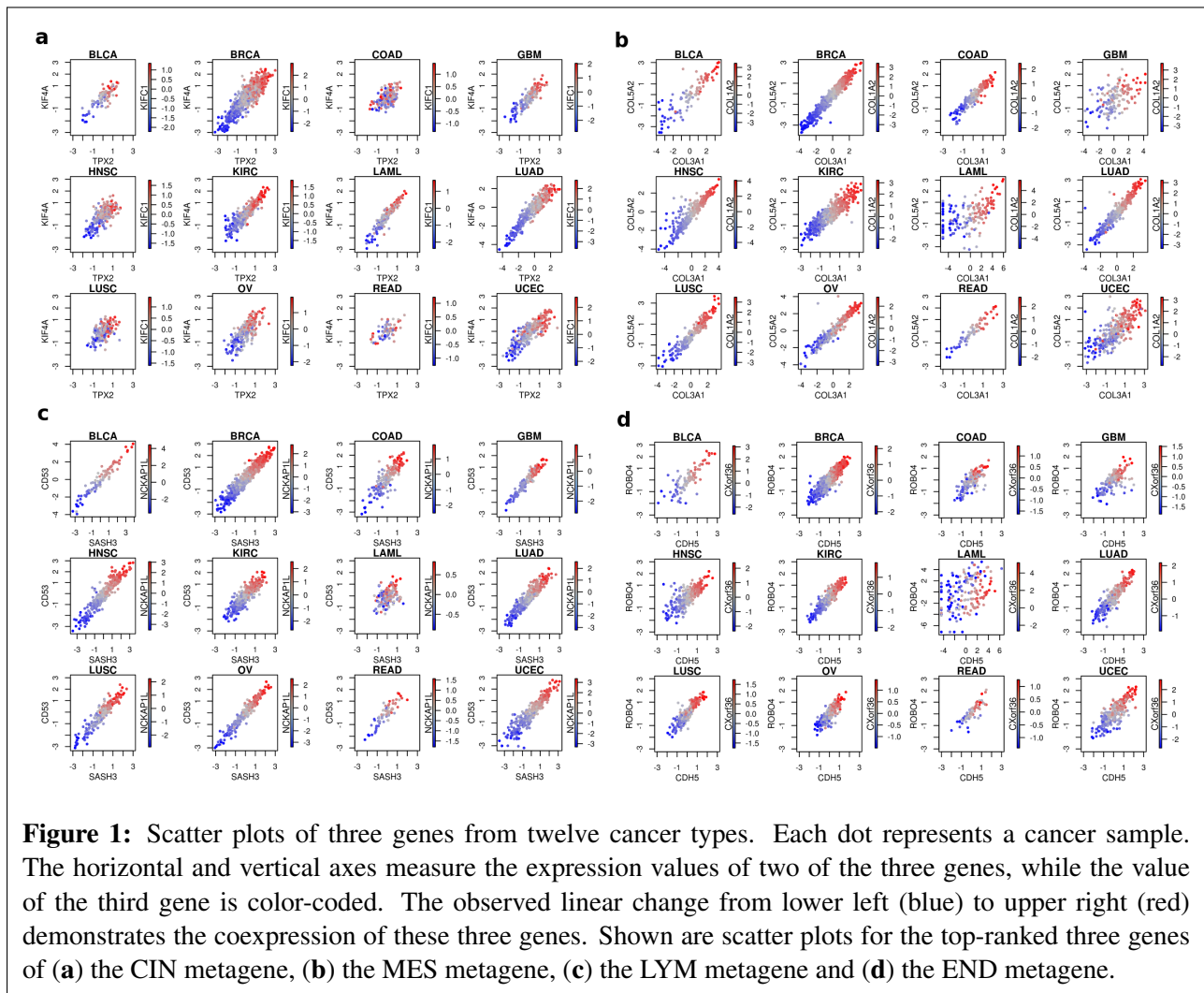


Table 1: Listing of the 18 attractor signatures

Name	Top members	Comments
mRNA		
LYM	<i>SASH3, CD53, NCKAP1L, LCP2, IL10RA, PTPRC, EVI2B, BIN2, WAS, HAVCR2</i>	lymphocyte infiltration
CIN	<i>TPX2, KIF4A, KIFC1, NCAPG, BUB1, NCAPH, CDCA5, KIF2C, PLK1, CENPA</i>	mitotic chromosomal instability
MES	<i>COL3A1, COL5A2, COL1A2, THBS2, COL5A1, VCAN, COL6A3, SPARC, AEBP1, FBN1</i>	mesenchymal transition

Continued on next page...

Table1 – continued from previous page

Name	Top members	Comments
END	<i>CDH5, ROBO4, CXorf36, CD34, CLEC14A, ARHGEF15, CD93, LDB2, ELTD1, MYCT1</i>	endothelial markers
“AHS2”	<i>AHSA2, LOC91316, PILRB, ZNF767, TTLL3, CCNL2, PABPC1L, LENG8, CHKB CPT1B, SEC31B</i>	
IFIT	<i>IFIT3, MX1, OAS2, RSAD2, CMPK2, IFIT1, IFI44L, IFI44, IFI6, OAS1</i>	interferon-induced
“WDR38”	<i>WDR38, YSK4, ROPN1L, C1orf194, MORN5, WDR16, RSPH4A, FAM183A, ZMYND10, DNAIL1</i>	
Genomically co-localized mRNA		
MHC Class II	<i>HLA-DPA1, HLA-DRA, HLA-DPB1, HLA-DRB1, HLA-DMA, HLA-DMB, HLA-DOA, HLA-DQA1, HLA-DRB5</i>	strongly associated with LYM
GIMAP cluster	<i>GIMAP4, GIMAP7, GIMAP6, GIMAP5, GIMAP8, GIMAP1</i>	strongly associated with LYM
Chr8q24.3 amplicon	<i>SHARPIN, HSF1, TIGD5, GPR172A, ZC3H3, EXOSC4, SCRIB, CYHR1, MAF1, PUF60</i>	most prominent Pan-Cancer amplicon
microRNA		
<i>DLK1-DIO3</i> RNA cluster	mir-127, mir-134, mir-379, mir-409, mir-382, mir-758, mir-381, mir-370, mir-654, mir-431	includes <i>MEG3</i> long noncoding RNA; associated with MES
“mir-509”	mir-509, mir-514, mir-508	
“mir-144”	mir-144, mir-451, mir-486	associated with erythropoiesis
Methylation		
“RMND1”	RMND1-6-151814639, MAP3K7-6-91353911, DNAAF1-16-82735714, PTRH2-17-55139429, ZNF143-11-9439170, cg03627896, TAMM41-3-11863582, CDK5-7-150385869, OTUB1-11-63510174, AATF-17-32380976	
M+	cg13928306, MTMR11-1-148175405, cg27324619, TNKS1BP1-11-56846646, C11orf52-11-111294703, IL17RC-3-9934128, cg24765079, ERBB3-12-54759072, IL22RA1-1-24342151, C11orf52-11-111294903	methyated in infiltrating lymphocytes

Continued on next page...

Table1 – continued from previous page

Name	Top members	Comments
M-	BIN2-12-50003941, PTPRCAP-11-66961771, TNFAIP8L2-1-149395922, IGFLR1-19-40925164, FAM113B-12-45896487, CD6-11-60495754, KLHL6-3- 184755939, PTPN7-1-200396189, FAM78A-9-133141340, ACAP1-17-7180947	Unmethylated in in- filtrating lymphocytes, may be causal to the expression of some of the genes of the LYM signature
Protein activity		
“c-Met”	c-Met, Snail, PARP_cleaved, Caspase-8, ERCC1, Rb	Related to apoptosis
“Akt”	Akt, Tuberin, STAT5A	

Lymphocyte infiltration: LYM mRNA signature; M+ methylation signature; M- methylation signature

These three signatures are related to tumor infiltration by lymphocytes. We list them together because they are strongly interrelated (**Fig. 2**) even though each of the three was independently derived using an unsupervised computational method. The presence of LYM is accompanied by the presence of M+ and the absence of M- in all solid cancer types, suggesting that the three signatures reflect the same biomolecular event, which appears to be the infiltration of immune cells in tumor tissue. Indeed, there is remarkable similarity (**Fig. 3**) between the LYM signature and the “immune score” of the ESTIMATE tumor purity computational tool (<http://ibl.mdanderson.org/estimate>). The values of the M+ methylation signature are also remarkably similar to those of the methylation-based “leukocyte percentage” estimation⁶ (available under Synapse ID syn1809222).

We had previously found⁷ all three LYM, M+ and M- signatures from their association with the expression of miR-142. We have now confirmed this association with miR-142 in the pancan12 data sets, and we found that miR-150 and miR-155 are also strongly associated with the LYM signature. We had also previously independently identified the LYM signature as an attractor metagene³, and used it in the winning model of the Sage Bionetworks Breast Cancer Prognosis Challenge⁴. Specifically the LYM signature is strongly associated with improved prognosis in ER-negative breast cancers, and this fact also provides an explanation for the relatively better prognosis in medullary, compared with other types of high-grade breast cancers.

The interrelationship of the LYM, M+ and M- signatures, as shown in **Fig. 2**, appears to be a consequence of the presence of different subclasses of cells (as opposed to being a methylation switch inside the same cell), consistent with their assumed role of measuring the extent of lymphocyte infiltration in the tumor. In other words, the M+ methylation sites, normally

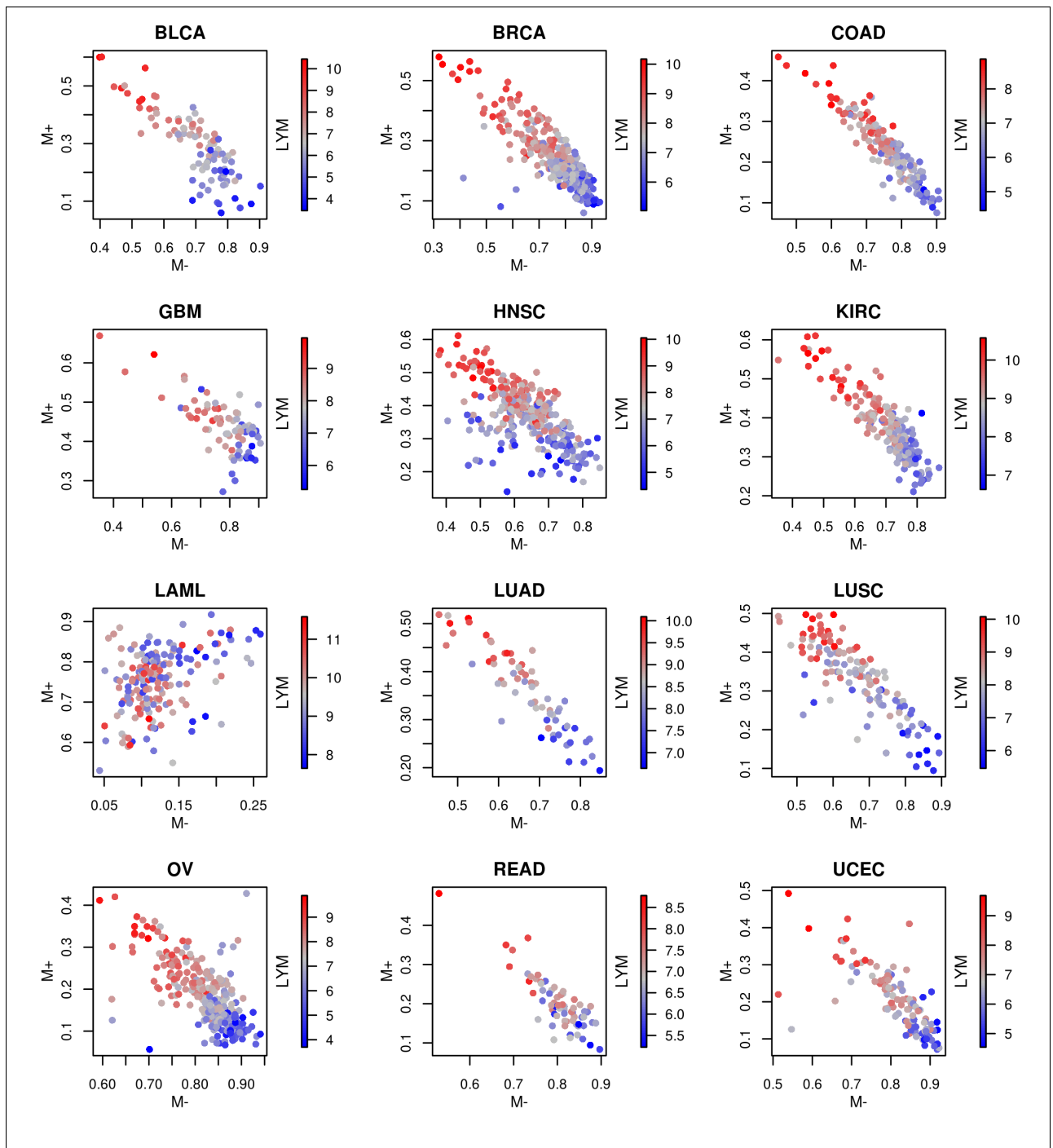


Figure 2: Scatter plots connecting the LYM, M+ and M- metagenes in 12 cancer types. Each dot represents a cancer sample. The horizontal and vertical axes measure the average methylation values of the two methylation signatures, M- and M+, while the value of the expression of the LYM metagene is color-coded. In all three cases, the metagene is defined by the average of the top ranked genes as described in **Table S1**.

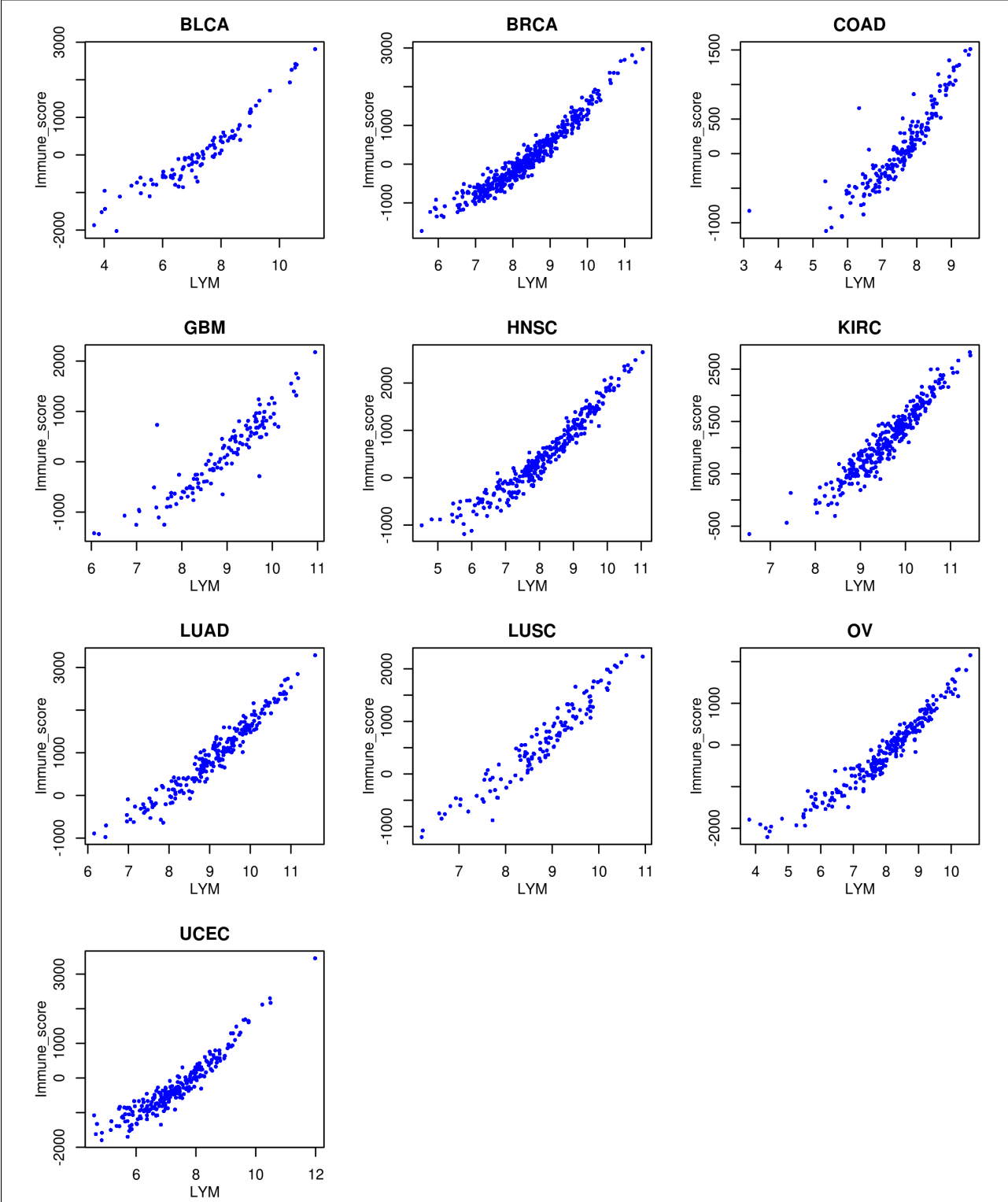


Figure 3: Scatter plots demonstrating the pan-cancer similarity of the value of the LYM metagene with the immune score of the ESTIMATE tumor purity computational tool (<http://ibl.mdanderson.org/estimate>) measuring immune cell infiltration. Each dot represents a cancer sample. The horizontal axis measures the expression value of the LYM metagene and the vertical axis measures the ESTIMATE immune score of infiltration. Note that the ESTIMATE did not provide scores for rectum cancer, and the estimation of immune cell infiltration is not applicable in leukemia.

unmethylated, are largely methylated in the infiltrating leukocytes; and the M- methylation sites, normally methylated, are largely unmethylated in the infiltrating leukocytes. Consistently, many of the genes methylated by the M- signature are identical to those of LYM (six among the 27 genes of the M- signature (*BIN2*, *TNFAIP8L2*, *ACAP1*, *NCKAP1L*, *FAM78A*, *PTPN7*) listed in Table S1 are also among the 168 genes listed in the LYM attractor metagene ($P < 9.21 \times 10^{-7}$ based on Fishers exact test). The observed significant overlap in the gene sets and the negative association between gene expression in LYM and DNA methylation in M- are consistent with the notion that the absence of DNA methylation is permissive for gene expression, suggesting that the expression of the LYM signature in the infiltrating lymphocytes may be facilitated in part by the hypomethylation of the M- signature.

The sharp definition of the LYM signature (being a Pan-Cancer attractor signature pointing to few genes at the core of coexpression) provides strong hints about the precise nature of this leukocyte infiltration. Specifically, the membership of the top-ranked genes (*SASH3*, *CD53*, *NCKAP1L*, *LCP2*, *IL10RA*, *PTPRC*, *EVI2B*, *BIN2*, *WAS*, *HAVCR2*, ...) point to a specific type of lymphocytes. We have speculated³ that these infiltrating lymphocytes are T cells having undergone a particular type of co-stimulation providing hypotheses for related adoptive transfer therapy.

Two proteins strongly associated with the LYM signature are two tyrosine kinases: Lck (lymphocyte-specific protein tyrosine kinase) and Syk (spleen tyrosine kinase).

CIN (mitotic chromosomal instability) mRNA signature

This signature is related to mitotic chromosomal instability. It is similar to numerous known “proliferation” signatures, but its sharp definition as an attractor metagene specifically points to the kinetochore-microtubule interface and associated kinesins. Comparison with similar mitotic signatures in normal cells may help pinpoint driver genes for malignant chromosomal instability. The signature is strongly associated with tumor grade as well as poor prognosis in many, if not all, cancer types.

Two proteins strongly associated with the CIN signature are Cyclin B1 and CDK1. Consistently, it is known that the cyclin B1-Cdk1 complex of cyclin-dependent kinase 1 is involved in the early events of mitosis, and that nuclear cyclin B1 protein may induce chromosomal instability and enhance the aggressiveness of the carcinoma cells⁸.

MES (mesenchymal transition) mRNA signature

This signature is related to mesenchymal transition and invasiveness of cancer cells. It is similar to numerous “stromal” or “mesenchymal” signatures; however there is evidence⁹ that many among the genes of the signature are largely produced by transdifferentiated cancer cells. We hypothesize that such cells, known to assume the duties of cancer-associated fibroblasts in some tumors², may have become indistinguishable, even using laser capture microdissection, from

stromal fibroblasts. We had originally identified the MES signature from its association with tumor stage¹⁰; specifically the signature appears only after a particular cancer type-specific tumor stage threshold has been reached.

The values of the MES signature are remarkably similar to the “stromal score” of the ESTIMATE tumor purity computational tool (<http://ibl.mdanderson.org/estimate>) measuring fibroblast infiltration. Based on our previous reasoning, however, we believe that this interpretation may not be fully accurate, and that it will be important to find out to what extent some of the cells expressing some of these mesenchymal markers may actually be transdifferentiated cancer cells, and whether the estimated tumor purity may be affected by other types of normal cells instead of stromal fibroblasts.

The co-regulated microRNAs most strongly associated with the MES signature are miR-199a, miR-199b, and miR-214. The *DLK1-DIO3* RNA cluster attractor signature, described later, is also strongly associated with MES.

The protein most strongly associated with the MES signature is Fibronectin.

END (endothelial marker) mRNA signature

This is a novel angiogenesis-associated attractor signature. Nearly all the top-ranked genes (**Table 1**) are endothelial markers. The top gene, *CDH5*, codes for VE-cadherin, which is known to be involved in a pathway suppressing angiogenic sprouting¹¹. The second gene, *ROBO4*, is known to inhibit VEGF-induced pathologic angiogenesis and endothelial hyperpermeability¹². Consistently, the END attractor metagene appears to be protective and anti-angiogenic, stabilizing the vascular network. For example, 22 out of the 27 genes of the END attractor are among the 265 genes included in File S2 of a recent study¹³ of renal cell carcinoma ($P < 8.4 \times 10^{-38}$ based on Fishers exact test) as most associated with patients survival. These good-prognosis genes were intermixed in the same file with many poor-prognosis genes of the CIN attractor, suggesting that the CIN and END attractor metagenes are two of the most prognostic features in renal cell carcinoma.

Interestingly, the MES and END attractor metagenes are positively associated with each other (**Fig. 4**), in the sense that overexpression of the END signature tends to imply overexpression of the MES signature and vice-versa. This is consistent with mutual exclusivity between angiogenesis and invasiveness and with related findings¹⁴ that VEGF inhibits tumor cell invasion and mesenchymal transition, while antiangiogenic therapy is associated with increased invasiveness¹⁵. It may also explain the paradoxical protective nature of signatures related to the MES attractor metagene in invasive breast cancers¹⁶.

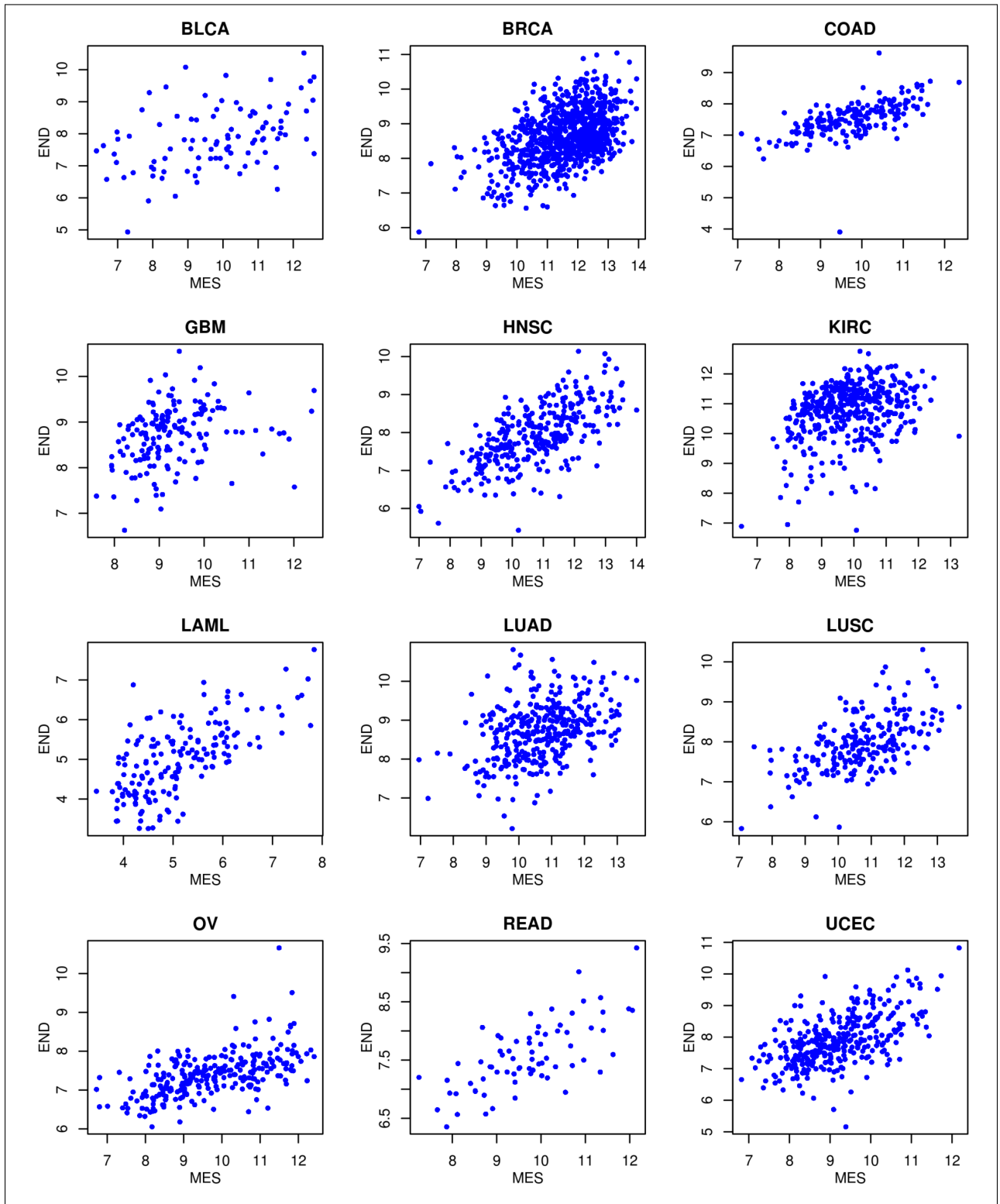


Figure 4: Scatter plots demonstrating the association between MES and END attractor metagenes. The horizontal and vertical axes measure the values of the MES and END signatures. The two signatures have positive correlation, although this association is not sufficiently strong to merge the two attractors into one. This association suggests that the invasive MES signature and the antiangiogenic END signature tend to be present simultaneously.

“AHS2” mRNA signature

We do not yet know what this signature represents. We observed that several noncoding RNAs (e.g. NCRNA00105, NCRNA00201) are in relatively high-ranked positions among its members.

IFIT (interferon-induced) mRNA signature

The members of this signature are interferon-induced. For example, we observed large enrichment of the genes of the signature among those upregulated by IFN- α in the side population (SP) of ovarian cancer cells¹⁷ from the list provided in Supplementary Table S4 of that paper, in which the authors concluded that tumors bearing large SP numbers could be particularly sensitive to IFN- α treatment.

“WDR38” mRNA signature

We do not know what this signature represents, except that we had found one of its key members, gene *ZMYND10*, to be protective and associated with estrogen receptor expression in breast cancer.

MHC Class II genomically co-localized mRNA signature

We found this signature using the genomically co-localized version of the algorithm. It is very highly correlated with LYM.

GIMAP genomically co-localized mRNA signature

As above, we found this signature using the genomically co-localized version of the algorithm. It is also very highly correlated with LYM.

Chr8q24.3 amplicon mRNA signature

This is the strongest pan-cancer amplicon signature. It was previously found predictive of early relapse in ER-positive breast cancers¹⁸.

“RMND1” methylation signature

We do not yet know what the comethylation of the sites of this signature signifies.

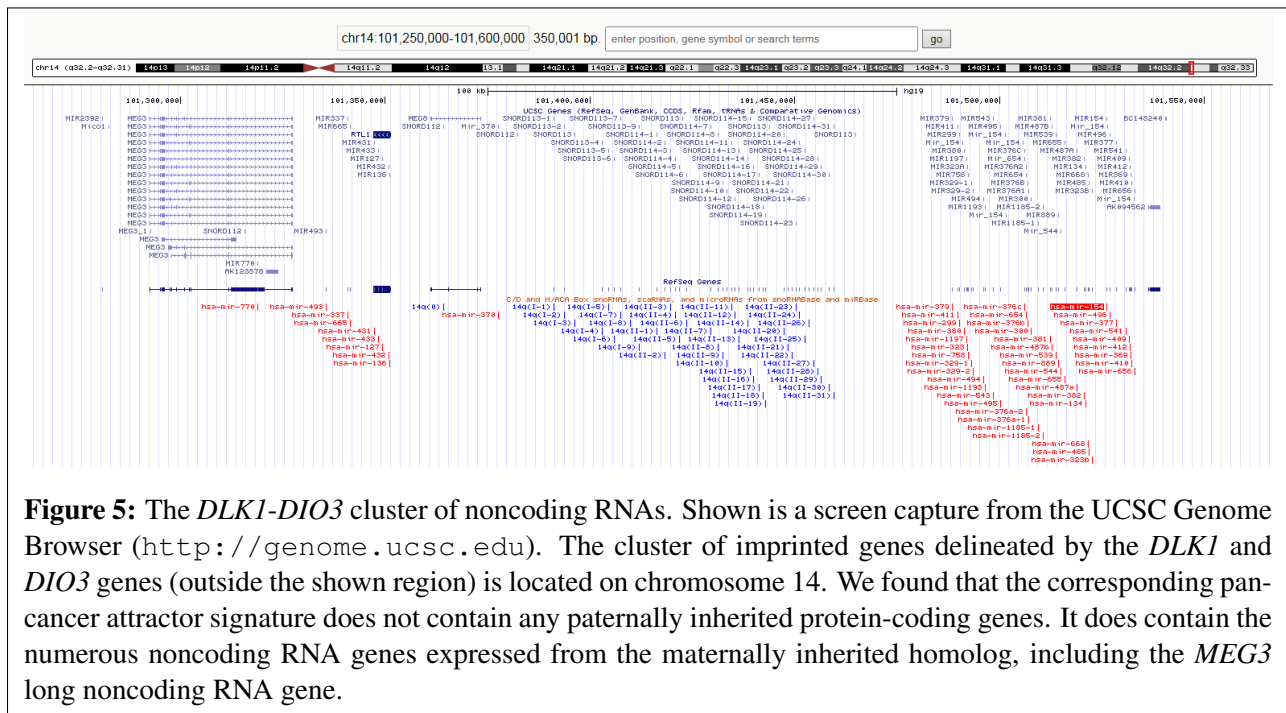


Figure 5: The *DLK1-DIO3* cluster of noncoding RNAs. Shown is a screen capture from the UCSC Genome Browser (<http://genome.ucsc.edu>). The cluster of imprinted genes delineated by the *DLK1* and *DIO3* genes (outside the shown region) is located on chromosome 14. We found that the corresponding pan-cancer attractor signature does not contain any paternally inherited protein-coding genes. It does contain the numerous noncoding RNA genes expressed from the maternally inherited homolog, including the *MEG3* long noncoding RNA gene.

***DLK1-DIO3* RNA cluster signature**

This is the strongest pan-cancer multi-microRNA coexpression signature. It consists of numerous noncoding RNAs within the *DLK1-DIO3* imprinted genomic region of chr14q32. **Fig. 5** shows a screen capture of the genomic region from the UCSC Genome Browser (<http://genome.ucsc.edu/>). We confirmed that the coexpression signature also includes the *MEG3* long noncoding RNA located at the upstream end of the region. It may also include numerous small nuclear RNAs at the central region, but there were no associated probe sets to confirm the coexpression. We found that this ncRNA signature is associated with the MES (mesenchymal transition) mRNA signature. For example, the ranked list of mRNAs most associated with the *DLK1-DIO3* ncRNA signature starts from *POSTN*, *PCOLCE*, *COL5A2*, *COL1A2*, *GLT8D2*, *COL5A1*, *SFRP2*, and *FAP*.

Expression of the imprinted *DLK1-DIO3* ncRNA cluster is believed to be vital for the development potential of embryonic stem cells¹⁹, consistent with the hypothesis²⁰ that mesenchymal transition in cancer reactivates embryonic developmental programs and makes cancer cells invasive and stem-like. The *DLK1-DIO3* ncRNA signature was also found to define a stem-like subtype of hepatocellular carcinoma associated with poor survival²¹. The details of the regulation mechanism for this ncRNA cluster coexpression in the *DLK1-DIO3* region are unclear.

“miR-509/miR-514/miR-508” microRNA signature

These three microRNAs are co-localized at chrXq27.3. We do not know what this signature signifies.

“miR-144/miR-451/miR-486” microRNA signature

This is a three-microRNA signature related to erythropoiesis. The first two genes are located in the bicistronic microRNA locus miR-144/451, highly expressed during erythrocyte development²². The mRNAs most associated to this microRNA signature are hemoglobin-related: *HBB*, *HBA1*, *HBA2* and *ALAS2*. The protein most associated with this signature is HER3. These three microRNAs were identified as promising biomarkers for detection of esophageal cancer.

c-Met/Snail/PARP_cleaved/Caspase-8/ERCC1/Rb protein activity signature

This protein coexpression signature appears to combine the contribution of several pathways and we hope that a plausible and useful biological “story” will be developed based on the simultaneous activity of all these six proteins in some cancer samples. We note that each of these proteins^{23–28} has been related in various ways with resistance to chemotherapy or apoptosis.

Akt/Tuberin/STAT5A protein activity signature

We do not know what the coexpression of Akt, Tuberin, STAT5A proteins represents in cancer. It is known, however, that low levels of STAT5A protein in breast cancer are associated with tumor progression and unfavorable clinical outcomes²⁹.

DISCUSSION

The Pan-Cancer nature (**Fig. S1**) of each of the signatures described in this paper suggests that they represent important biomolecular events. A reasonable concern is whether some of these “pan-cancer” signatures may instead reflect fundamental normal “pan-tissue” biological mechanisms. Even if this is true for some of these signatures, this does not exclude the possibility that they are aberrant and play important roles in some cancer samples. Furthermore, this provides the opportunity to compare similar signatures in normal vs. malignant tissues to pinpoint potential cancer-specific genes.

Because of its exhaustive search starting from all potential “seeds” in all data sets from twelve different cancer types, our iterative data mining algorithm is guaranteed to have identified all pan-cancer molecular signatures involving simultaneous presence of a large number of coordinately expressed genes, proteins, or comethylated sites. We hope that these signatures are further scrutinized by the medical research community for the purpose of developing potential diagnostic, predictive, and eventually therapeutic products applicable in multiple cancers.

ACKNOWLEDGEMENTS

We are thankful to Hanina Hibshoosh, Chris Miller and Gordon Mills for helpful discussions, which contributed to improved interpretation of the signatures disclosed in this paper.

Accessibility

All figures in this paper, including supplementary figures and tables, as well as the files of generated attractor molecular signatures, are available in Synapse under ID syn1686966.

Data description and availability

The data sets of TCGA pancan12 freeze 4.7 used to derive the results of this paper are described and are available under Synapse ID syn300013 with doi:10.7303/syn300013. The twelve cancer types are bladder urothelial carcinoma (BLCA), breast invasive carcinoma (BRCA), colon adenocarcinoma (COAD), glioblastoma multiforme (GBM), head and neck squamous cell carcinoma (HNSC), kidney renal clear cell carcinoma (KIRC), acute myeloid leukemia (LAML), lung adenocarcinoma (LUAD), lung squamous cell carcinoma (LUSC), ovarian serous cystadenocarcinoma (OV), rectum adenocarcinoma (READ), and uterine corpus endometrioid carcinoma (UCEC).

References

1. Hanahan, D. & Weinberg, R.A. The hallmarks of cancer. *Cell* 100, 57-70 (2000).
2. Hanahan, D. & Weinberg, R.A. Hallmarks of cancer: the next generation. *Cell* 144, 646-74 (2011).
3. Cheng, W.Y., Ou Yang, T.H. & Anastassiou, D. Biomolecular events in cancer revealed by attractor metagenes. *PLoS Comput Biol* 9, e1002920 (2013).
4. Cheng, W.Y., Ou Yang, T.H. & Anastassiou, D. Development of a prognostic model for breast cancer survival in an open challenge environment. *Sci Transl Med* 5, 181ra50 (2013).
5. McCarthy, N. Prognostic models: Rising to the challenge. *Nat Rev Cancer*, doi:10.1038/nrc3530 (2013).
6. Shen, H. *et al.* Comprehensive Cross-Cancer Comparison of DNA Methylation Profiles, submitted. (2013).
7. Andropoulos, B. & Anastassiou, D. Integrated Analysis Reveals hsa-miR-142 as a Representative of a Lymphocyte-Specific Gene Expression and Methylation Signature. *Cancer Inform* 11, 61-75 (2012).
8. Suzuki, T. *et al.* Nuclear cyclin B1 in human breast carcinoma as a potent prognostic factor. *Cancer Sci* 98, 644-51 (2007).
9. Anastassiou, D. *et al.* Human cancer cells express Slug-based epithelial-mesenchymal transition gene expression signature obtained in vivo. *BMC Cancer* 11, 529 (2011).
10. Kim, H., Watkinson, J., Varadan, V. & Anastassiou, D. Multi-cancer computational analysis reveals invasion-associated variant of desmoplastic reaction involving INHBA, THBS2 and COL11A1. *BMC Med Genomics* 3, 51 (2010).
11. Abraham, S. *et al.* VE-Cadherin-mediated cell-cell interaction suppresses sprouting via signaling to MLC2 phosphorylation. *Curr Biol* 19, 668-74 (2009).
12. Jones, C.A. *et al.* Robo4 stabilizes the vascular network by inhibiting pathologic angiogenesis and endothelial hyperpermeability. *Nat Med* 14, 448-53 (2008).
13. Wozniak, M.B. *et al.* Integrative genome-wide gene expression profiling of clear cell renal cell carcinoma in Czech Republic and in the United States. *PLoS One* 8, e57886 (2013).
14. Lu, K.V. *et al.* VEGF inhibits tumor cell invasion and mesenchymal transition through a MET/VEGFR2 complex. *Cancer Cell* 22, 21-35 (2012).
15. Paez-Ribes, M. *et al.* Antiangiogenic therapy elicits malignant progression of tumors to increased local invasion and distant metastasis. *Cancer Cell* 15, 220-31 (2009).

16. Beck, A.H., Espinosa, I., Gilks, C.B., van de Rijn, M. & West, R.B. The fibromatosis signature defines a robust stromal response in breast carcinoma. *Lab Invest* 88, 591-601 (2008).
17. Moserle, L. *et al.* The side population of ovarian cancer cells is a primary target of IFN-alpha antitumor effects. *Cancer Res* 68, 5658-68 (2008).
18. Bilal, E. *et al.* Amplified Loci on Chromosomes 8 and 17 Predict Early Relapse in ER-Positive Breast Cancers. *PLoS One* 7, e38575 (2012).
19. Stadtfeld, M. *et al.* Aberrant silencing of imprinted genes on chromosome 12qF1 in mouse induced pluripotent stem cells. *Nature* 465, 175-81 (2010).
20. Mani, S.A. *et al.* The epithelial-mesenchymal transition generates cells with properties of stem cells. *Cell* 133, 704-15 (2008).
21. Luk, J.M. *et al.* DLK1-DIO3 genomic imprinted microRNA cluster at 14q32.2 defines a stemlike subtype of hepatocellular carcinoma associated with poor survival. *J Biol Chem* 286, 30706-13 (2011).
22. Yu, D. *et al.* miR-451 protects against erythroid oxidant stress by repressing 14-3-3zeta. *Genes Dev* 24, 1620-33 (2010).
23. Tang, M.K., Zhou, H.Y., Yam, J.W. & Wong, A.S. c-Met overexpression contributes to the acquired apoptotic resistance of nonadherent ovarian cancer cells through a cross talk mediated by phosphatidylinositol 3-kinase and extracellular signal-regulated kinase 1/2. *Neoplasia* 12, 128-38 (2010).
24. Haslehurst, A.M. *et al.* EMT transcription factors snail and slug directly contribute to cisplatin resistance in ovarian cancer. *BMC Cancer* 12, 91 (2012).
25. DAmours, D., Sallmann, F.R., Dixit, V.M. & Poirier, G.G. Gain-of-function of poly(ADP-ribose) polymerase-1 upon cleavage by apoptotic proteases: implications for apoptosis. *J Cell Sci* 114, 3771-8 (2001).
26. Kim, P.K., Mahidhara, R. & Seol, D.W. The role of caspase-8 in resistance to cancer chemotherapy. *Drug Resist Updat* 4, 293-6 (2001).
27. Olaussen, K.A. *et al.* DNA repair by ERCC1 in non-small-cell lung cancer and cisplatin-based adjuvant chemotherapy. *N Engl J Med* 355, 983-91 (2006).
28. Collard, T.J. *et al.* The retinoblastoma protein (Rb) as an anti-apoptotic factor: expression of Rb is required for the anti-apoptotic function of BAG-1 protein in colorectal tumour cells. *Cell Death Dis* 3, e408 (2012).
29. Peck, A.R. *et al.* Low levels of Stat5a protein in breast cancer are associated with tumor progression and unfavorable clinical outcomes. *Breast Cancer Res* 14, R130 (2012).

METHODS

Data normalization

The data platform for each cancer types and its corresponding Synapse ID is given below.

Molecular profile	mRNA	Protein	miRNA	DNA methylation
Platform	Illumina HiSeq	Reverse phase protein lysate microarray (RPPA)	Illumina HiSeq	Infinium HumanMethylation27 BeadChip
Cancer type	Synapse ID			
BLCA	syn1571504	syn1681048	syn1571494	syn1889358*
BRCA	syn417812	syn1571267	syn395575	syn411485
COAD	syn1446197	syn416772	syn464211	syn411993
GBM	syn1446214	syn416777	NA	syn412284
HNSC	syn1571420	syn1571409	syn1571411	syn1889356*
KIRC	syn417925	syn416783	syn395617	syn412701
LAML	syn1681084	NA	syn1571533	syn1571536
LUAD	syn1571468	syn1571446	syn1571453	syn1571458
LUSC	syn418033	syn1367036	syn395691	syn415758
OV	syn1446264	syn416789	syn1356544	syn415945
READ	syn1446276	syn416795	syn464222	syn416194
UCEC	syn1446289	syn416800	syn395720	syn416204

* The data sets were extracted from HumanMethylation450 BeadChip.

For each RNA sequencing and miRNA sequencing data set, the mRNAs or miRNAs in which more than 50% of the samples have zero counts were removed from the data set. All the zero counts and missing values in the data sets were imputed using the k-nearest neighbors algorithm as implemented in the *impute* package in Bioconductor. The log2 transformed counts were then normalized using the quantile normalization methods implemented in Bioconductor's *limma* package. The missing values in the protein and DNA methylation data sets were also imputed using the k-nearest neighbors algorithm in the *impute* package. We summarized the miRNA expression values by taking the average expression values of the miRNAs with the same gene family names. For bladder and head and neck methylation data sets, for which only the Humanmethylation450 platform were provided, we extracted the 23,380 overlapping probes between the Humanmethylation27 and HumanMethylation450 platforms as new data sets for analysis.

Finding attractors

The iterative algorithm for finding converged attractors was previously described³ and is available as an R package under Synapse ID syn1123167. We used the same parameters as in our previous work. Specifically, we selected the value of the exponent a to be 5 for mRNA sequencing, and we used the same value for miRNA sequencing and for DNA methylation. For protein data sets due to their smaller dimension, the exponent was set to 2. For genomically co-localized mRNA

attractors, the parameters were set as previously defined³. The strength of an attractor (to be used for attractor ranking as described below) was defined as the k -th highest mutual information among all genes with the converged attractor. For mRNA and methylation attractors, we set $k = 10$, and for miRNA and protein attractors, we defined $k = 3$, because we observed that these attractors tend to consist of a smaller number of mutually associated elements.

Clustering attractors of different cancer types

After obtaining the converged attractors in each data set, we performed a clustering algorithm to identify extremely similar attractors across different cancer types, using the same algorithm as in our previous work³. We used the top features mRNAs, miRNAs, proteins, or methylation probes in each attractor as a feature set, then performed hierarchical clustering on the feature sets across the cancer types, using the number of overlapping features as the similarity measure. The number of top features used to represent the attractor was chosen according to the distribution of the features' weights in the attractors. For the mRNA attractors, we used the top 20 features to create such feature sets. For the methylation attractors, we used top 50 features for clustering. For the miRNA and protein attractors, we used the top five features for clustering. We removed a methylation attractor cluster containing sites exclusively on the X or Y chromosome, because we found that their values were gender-based. If an attractor cluster did not contain any gene that found in at least six cancer types, it was removed from consideration.

Creating consensus molecular signatures

To account for the fact that some of the twelve data sets may not contain sufficient heterogeneous samples for showing each Pan-Cancer biomolecular event, the decision of selecting a signature was based on its clear presence in at least half of the cancer types, *i.e.*, six different cancer types. We thus created a consensus molecular signature from each attractor cluster as follows: We first identified, for each cluster, six significant attractors by calculating the sum of the similarity measures (as defined above) between each attractor and all the other attractors, ranking the attractors using this quantity, and selecting the six top-ranked attractors. If an attractor cluster contained less than six attractors, it was removed from consideration. We then calculated the average score for each feature across the six attractors and ranked the features accordingly as the consensus ranking. The ranking of the features is provided in **Table S1**.

Data visualization

To create scatter plots for the top three features in the attractor, we median-centered the values of the features on both axes, so the median value for each feature in each data set is zero on the scatter plots. For the color-coded feature, we set the median to be gray, the minimum value to be blue, and the maximum value to be red, and interpolated the colors for intermediate values. For mRNA sequencing and miRNA sequencing data, the outlier values were removed, where the outliers were identified using the *boxplot* function in R.

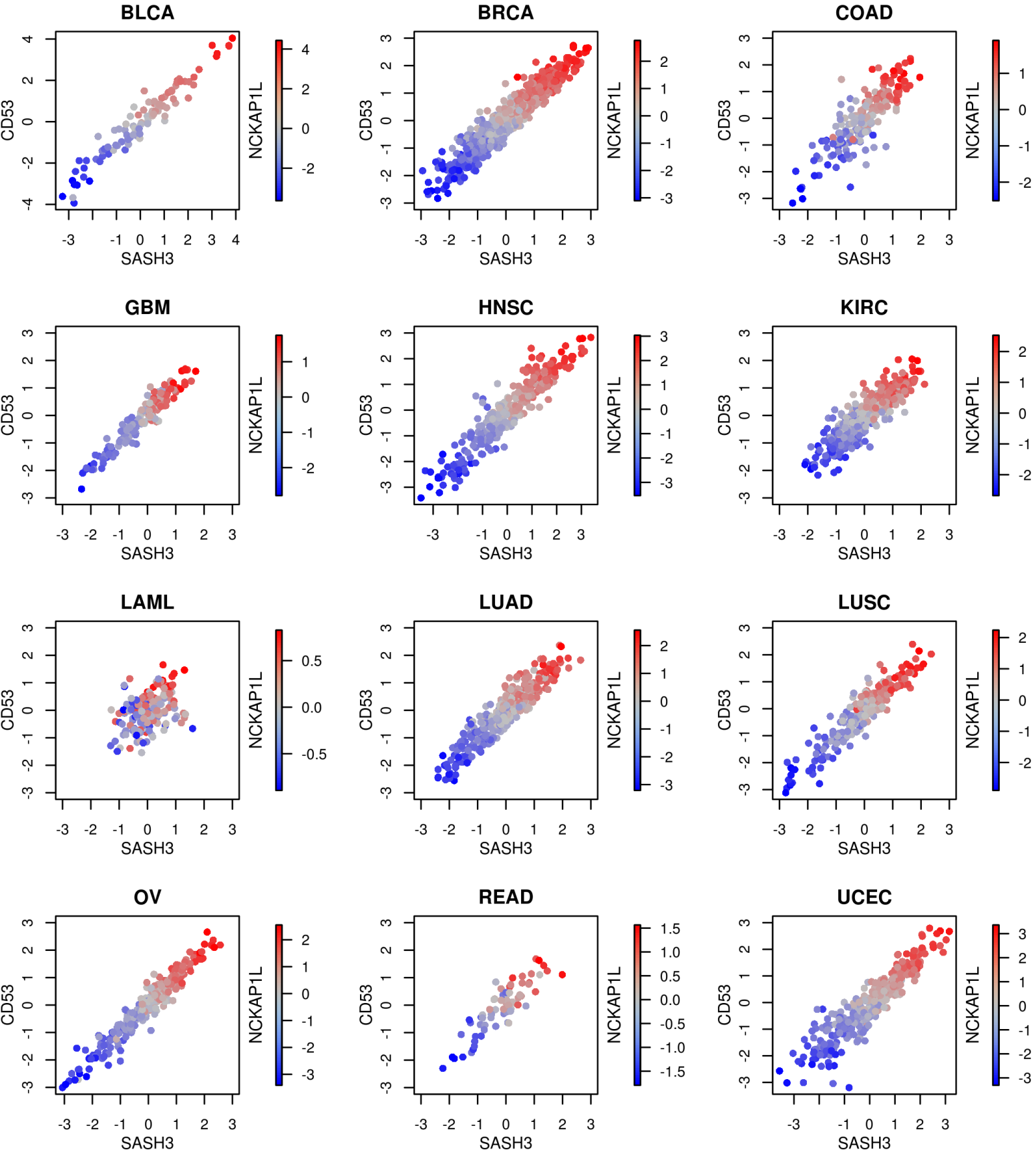
Ranking attractor clusters

The strength of an attractor cluster was defined as the average strength of the six selected attractors in the cluster, as identified in the previous section.

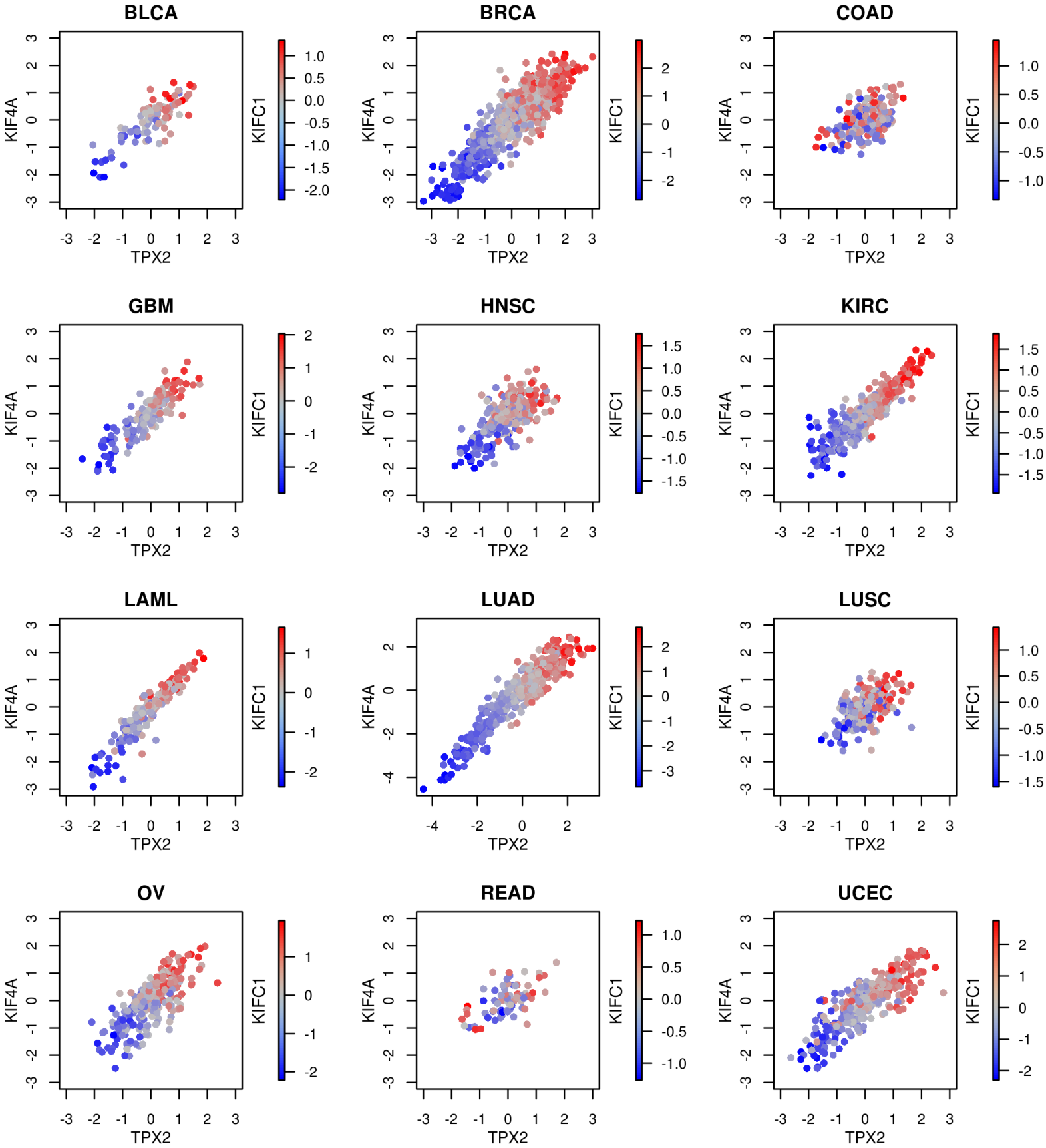
Supplementary Figures

Figure S1: Scatter plots of the top three features for each of the 15 molecular signatures, demonstrating strong mutual association in nearly all cases, with very few exceptions, usually in leukemia. Each dot represents a cancer sample. The horizontal and vertical axes measure the values of two of the three features, while the value of the third feature is color-coded from blue to red.

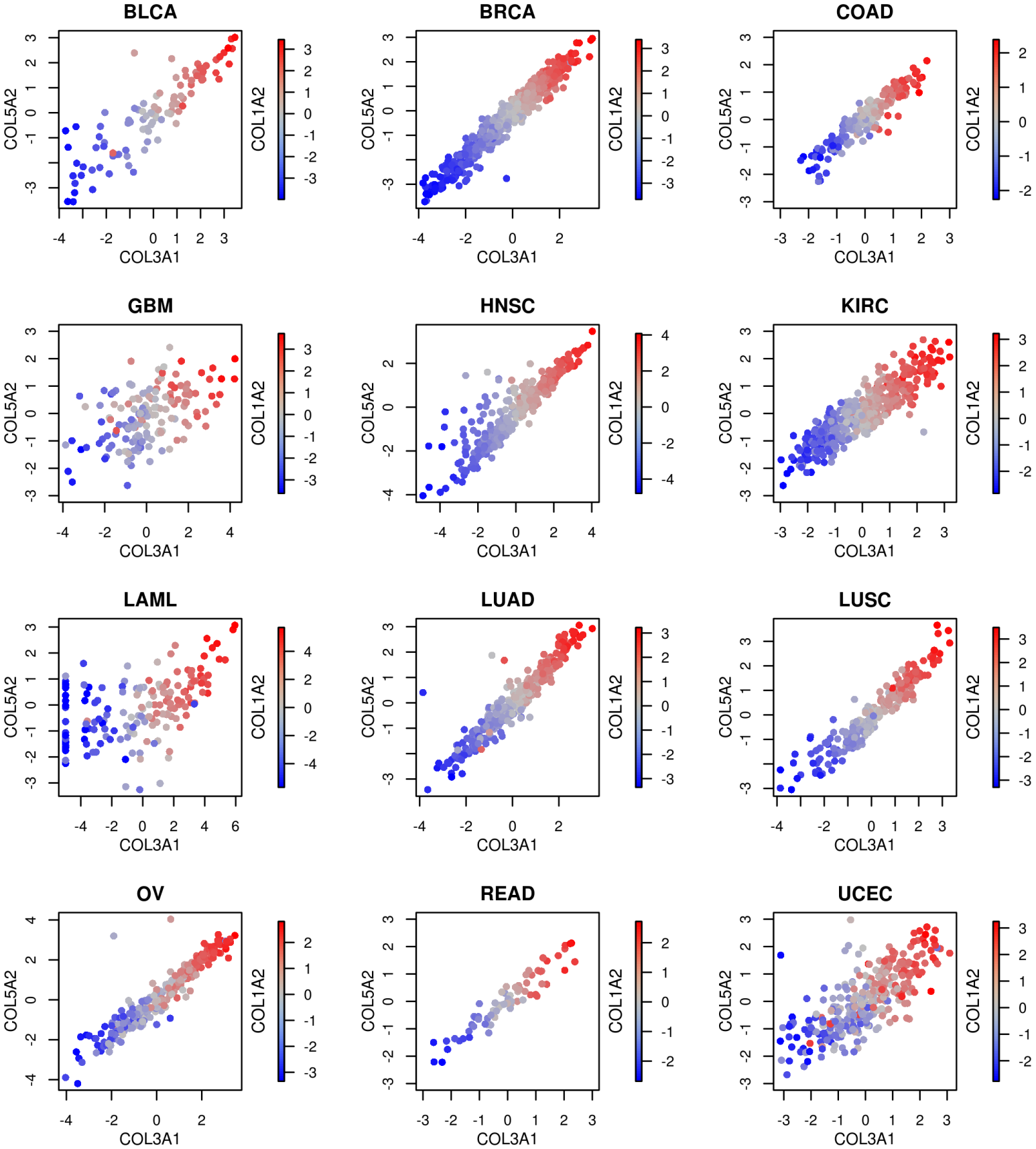
1. LYM mRNA attractor



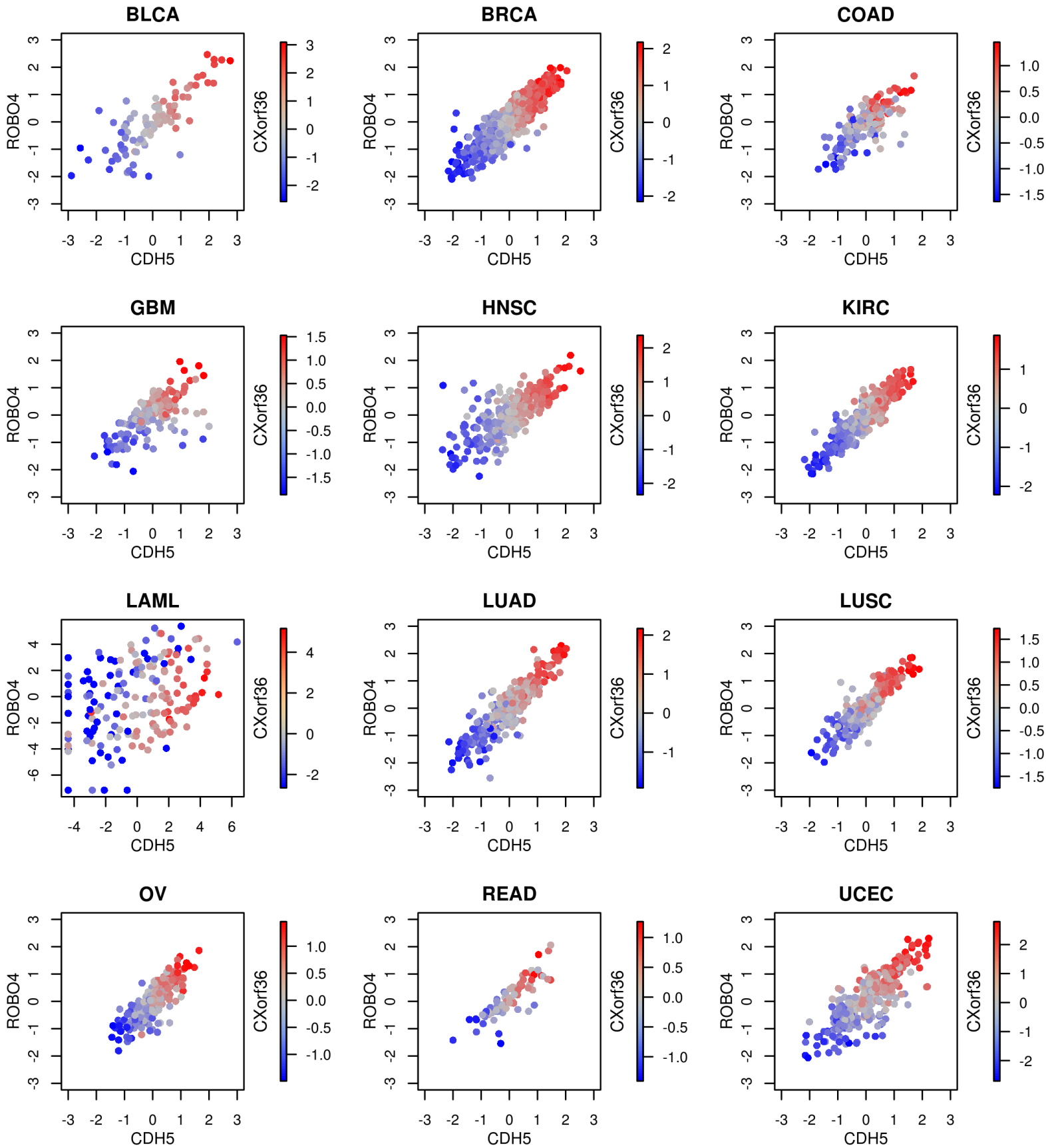
2. CIN mRNA attractor



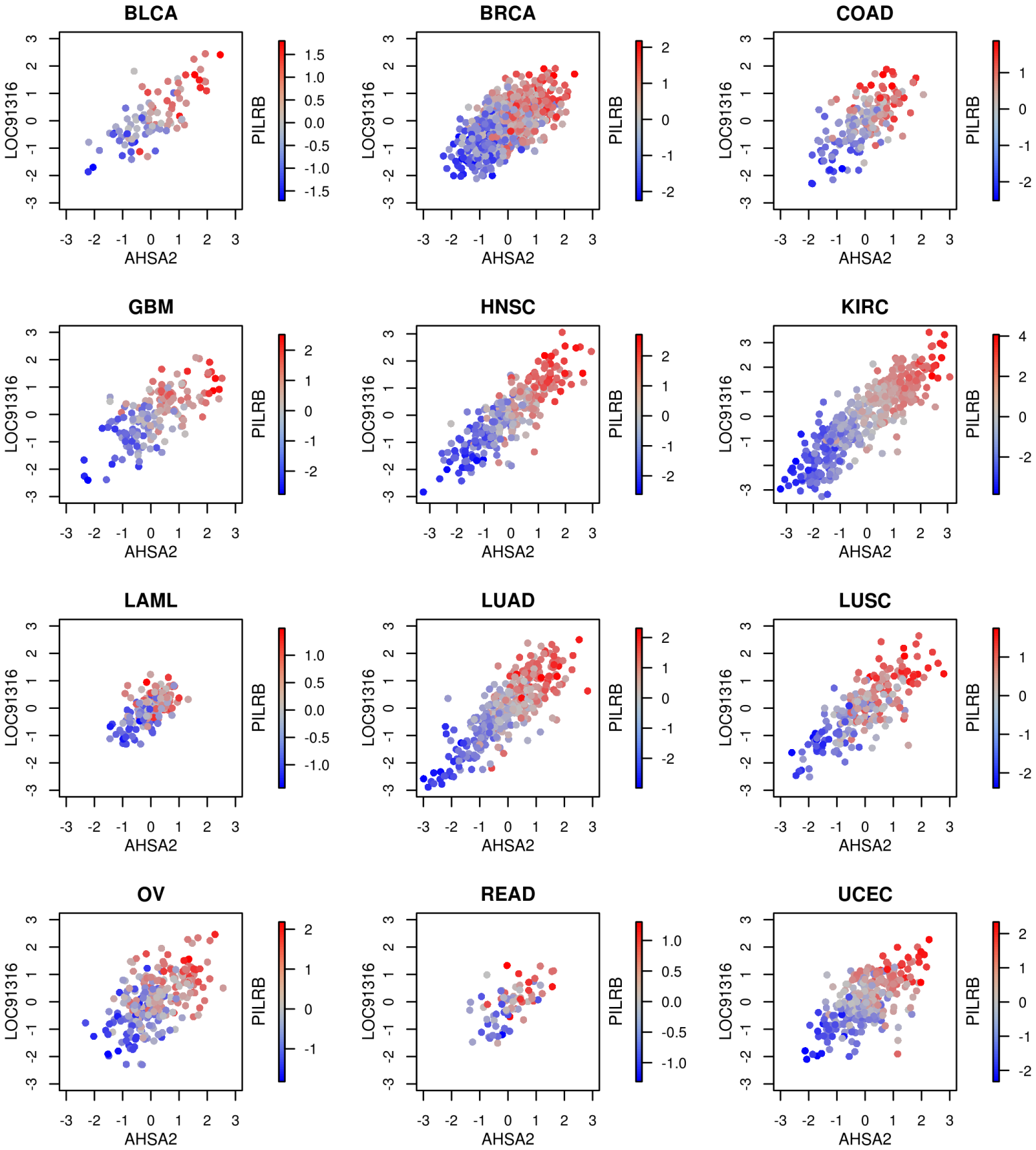
3. MES mRNA attractor



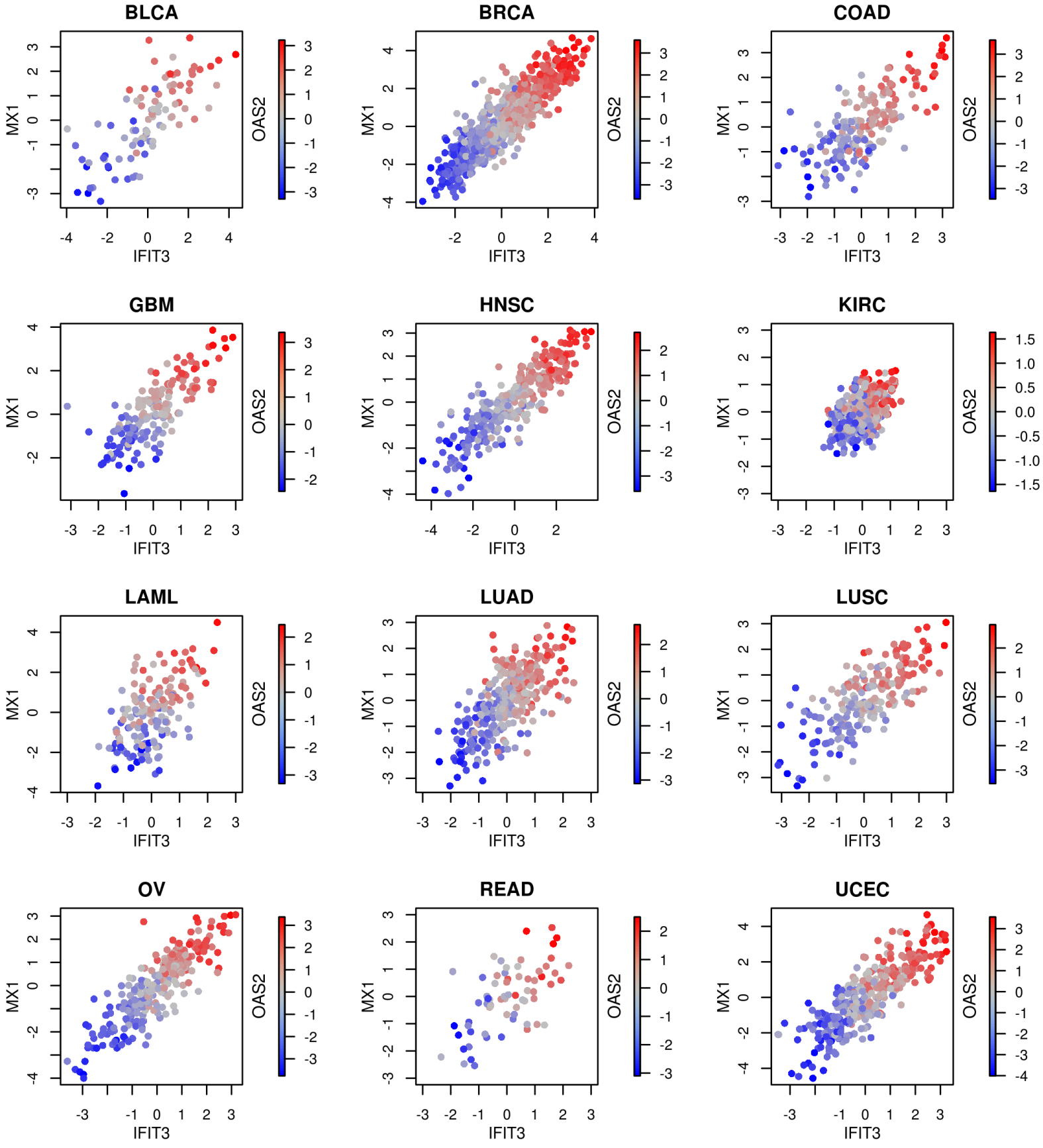
4. END mRNA attractor



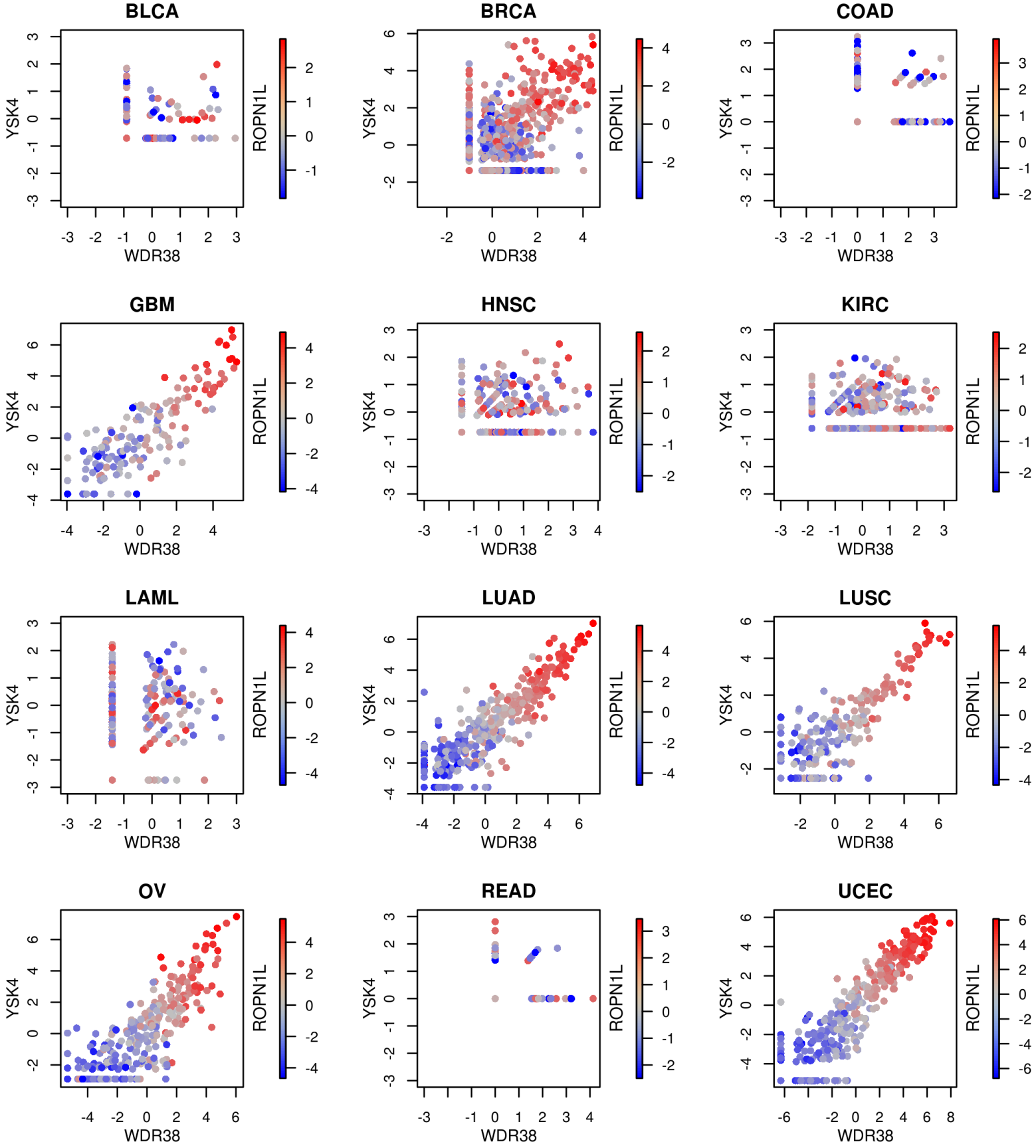
5. AHSA2 mRNA attractor



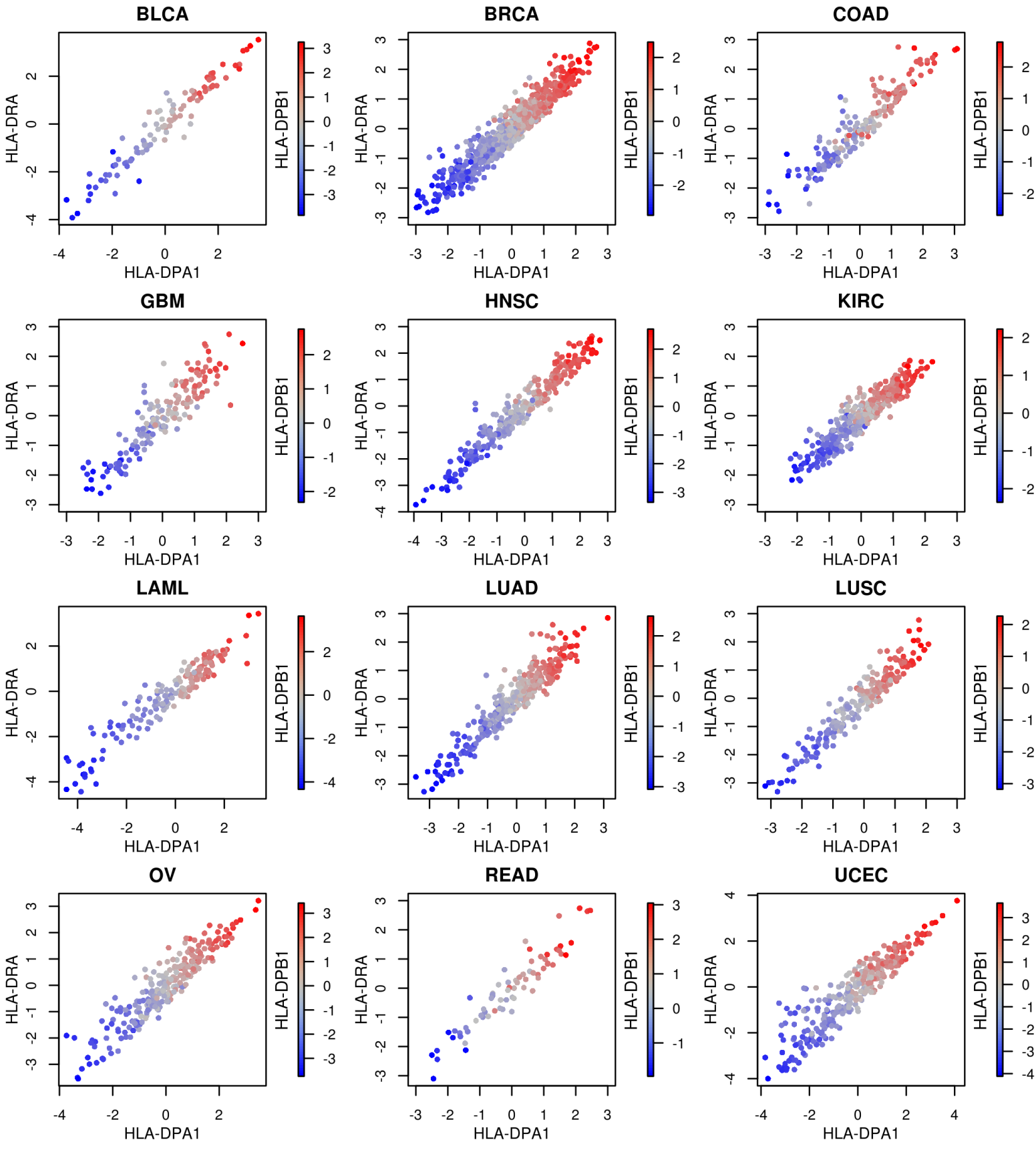
6. IFIT mRNA attractor



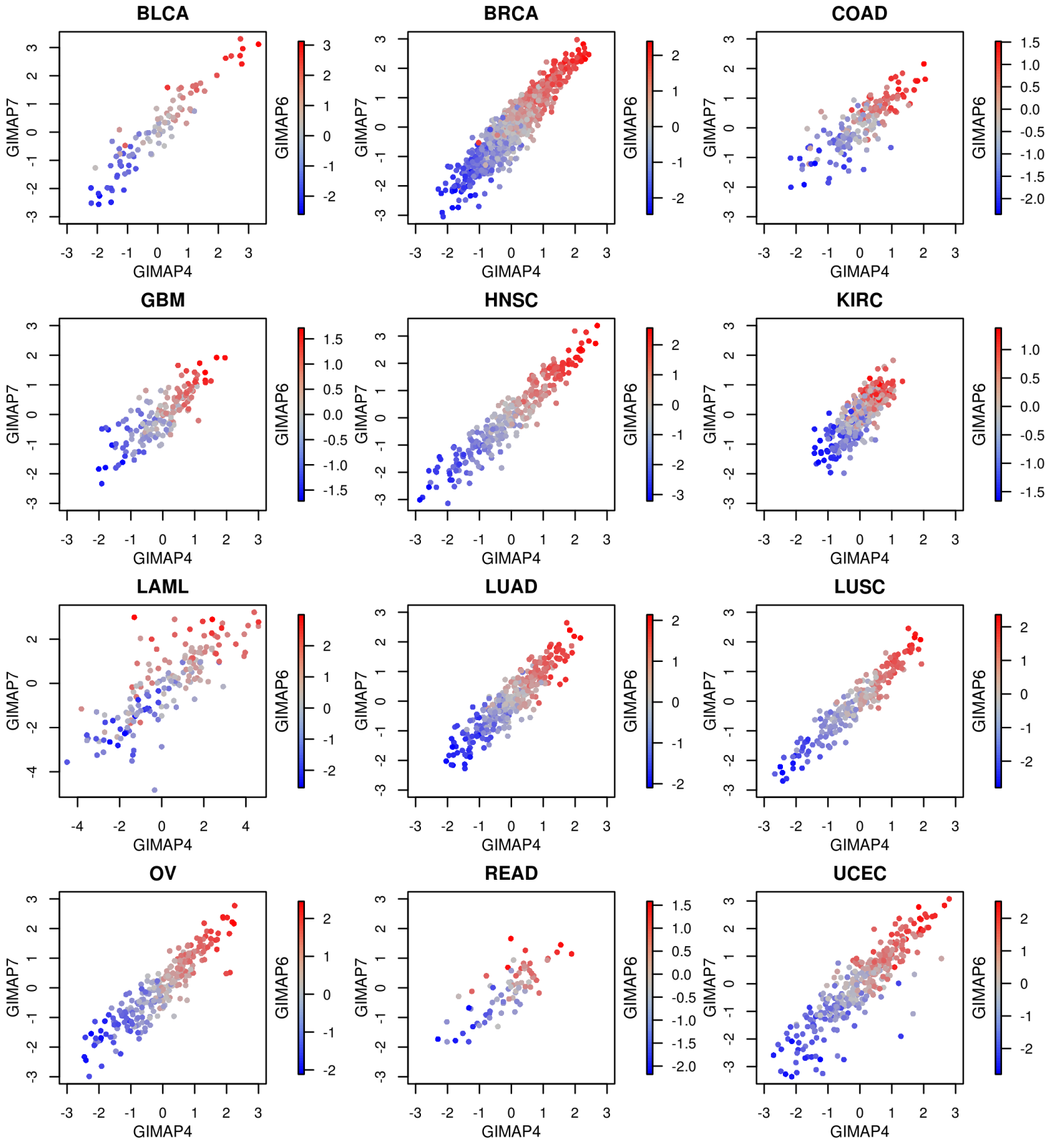
7. WDR38 mRNA attractor



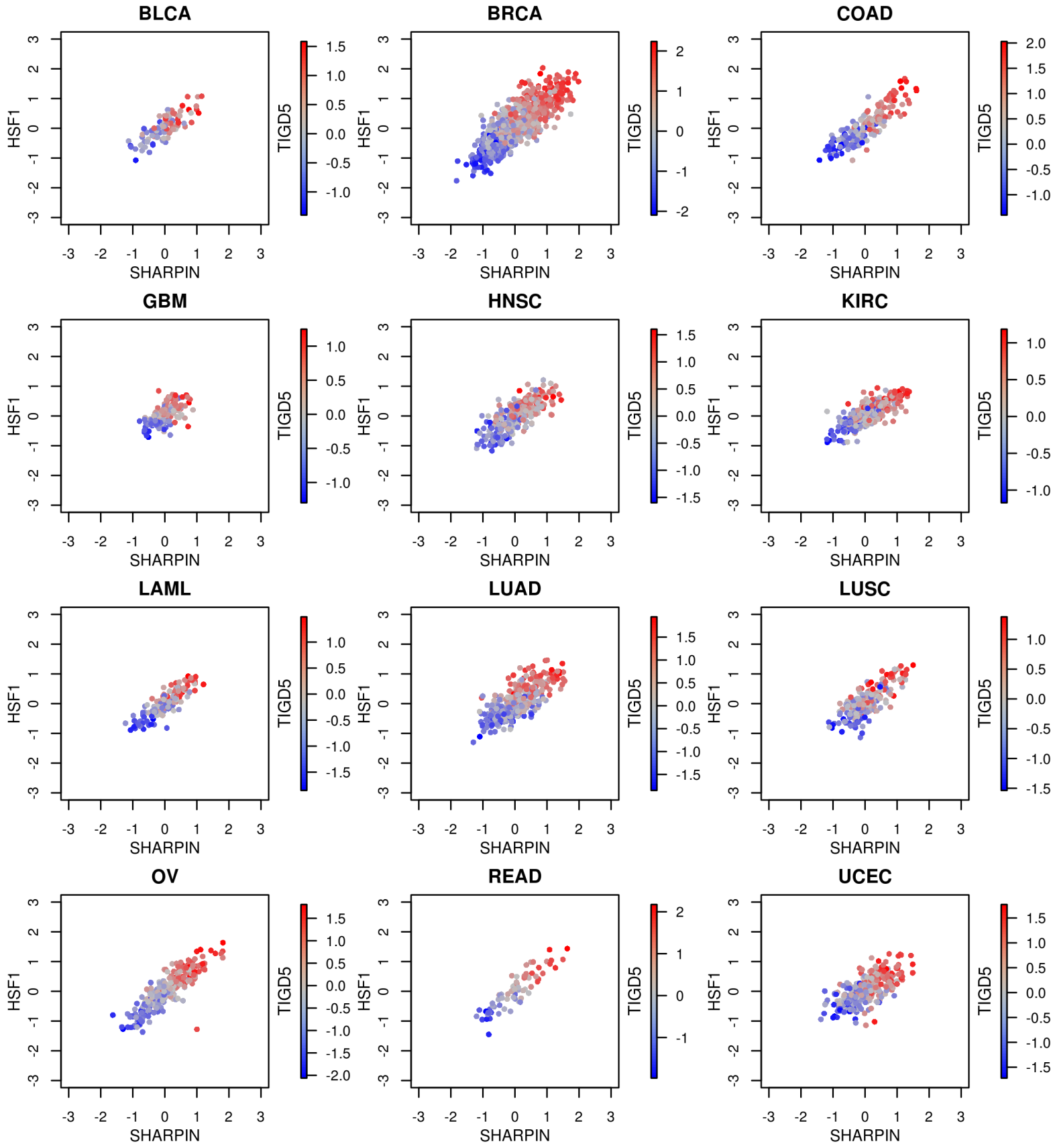
8. MHC Class II



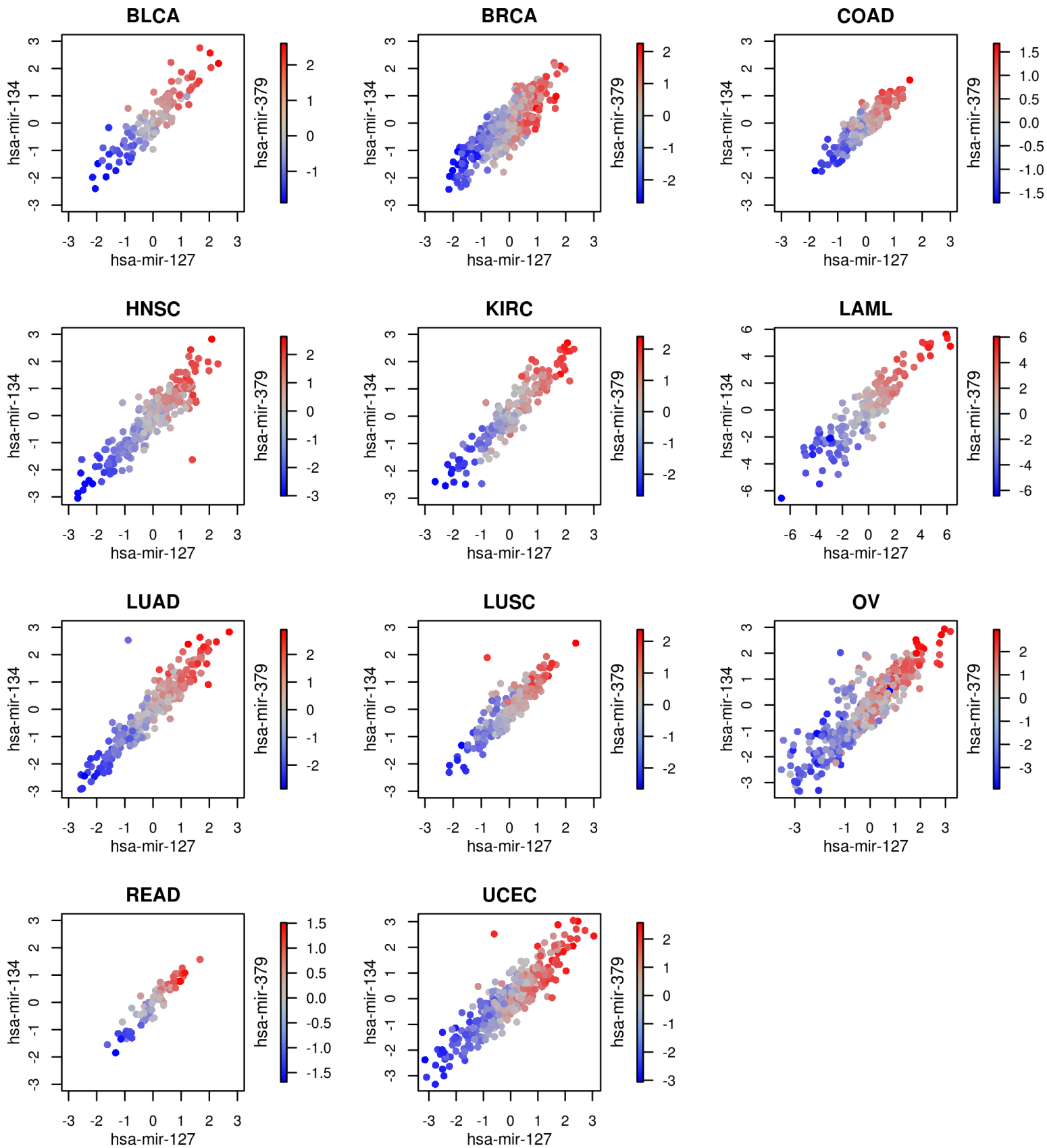
9. GIMAP cluster



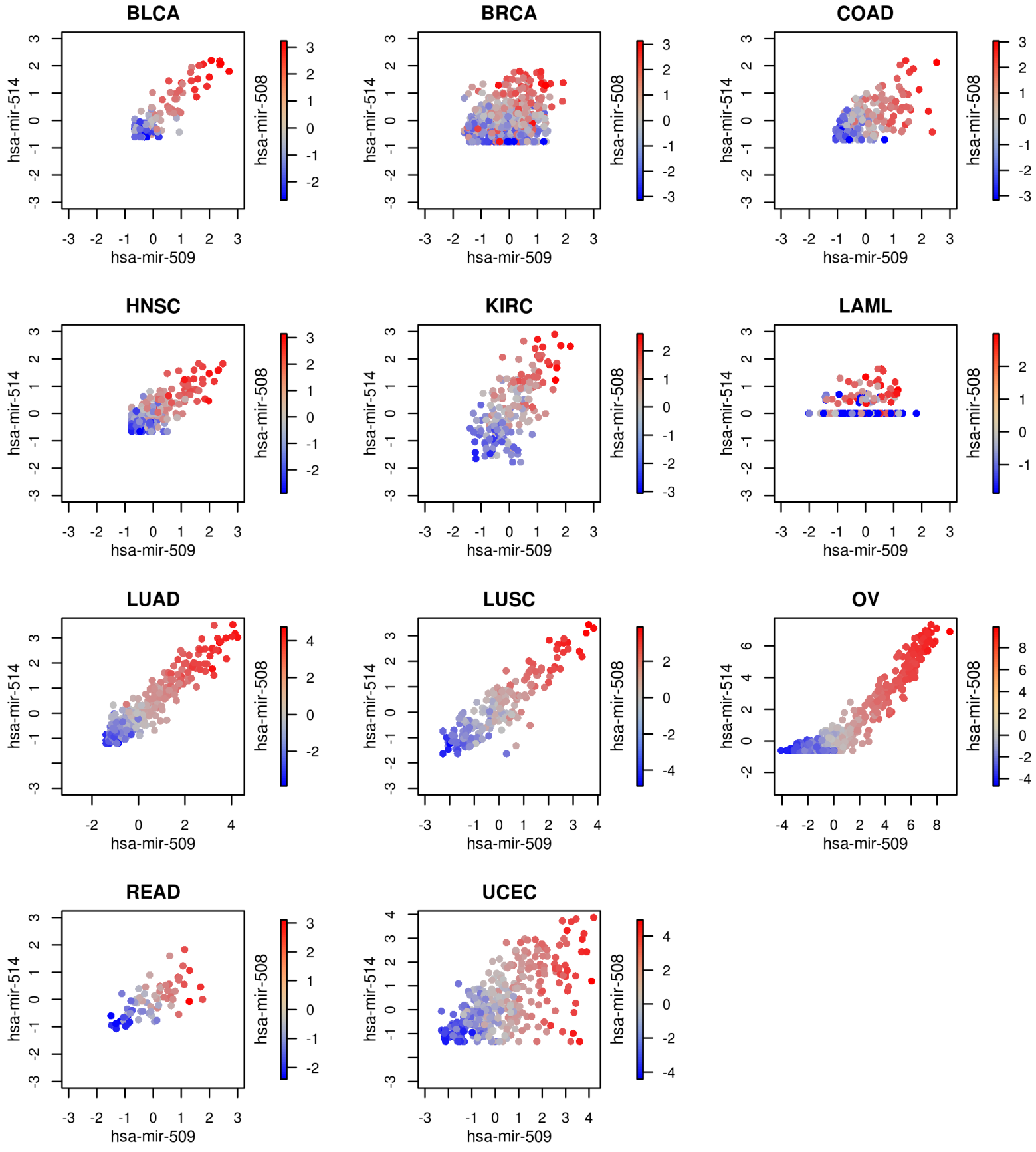
10. Chr8q24.3 amplicon



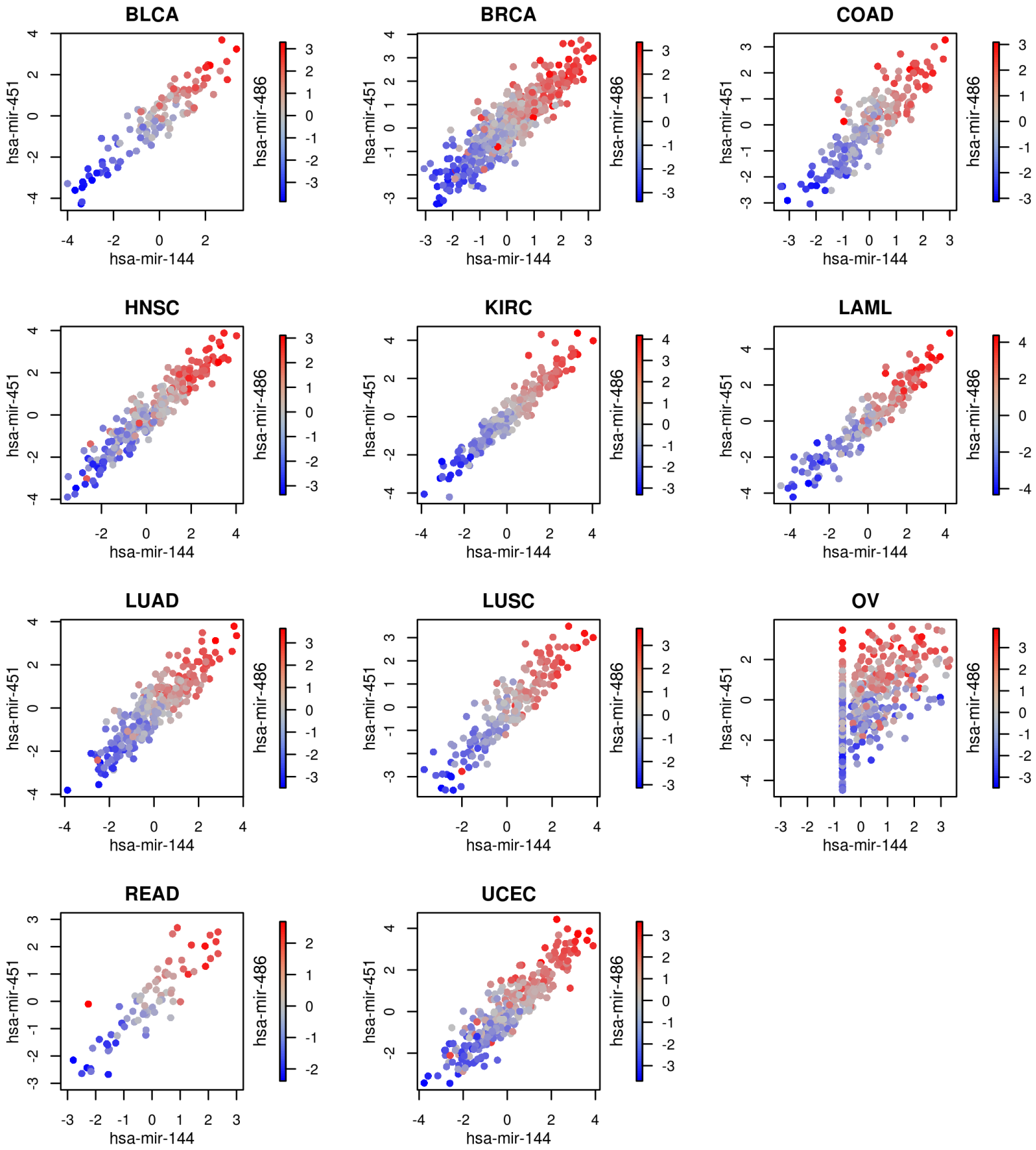
11. mir127 miRNA attractor



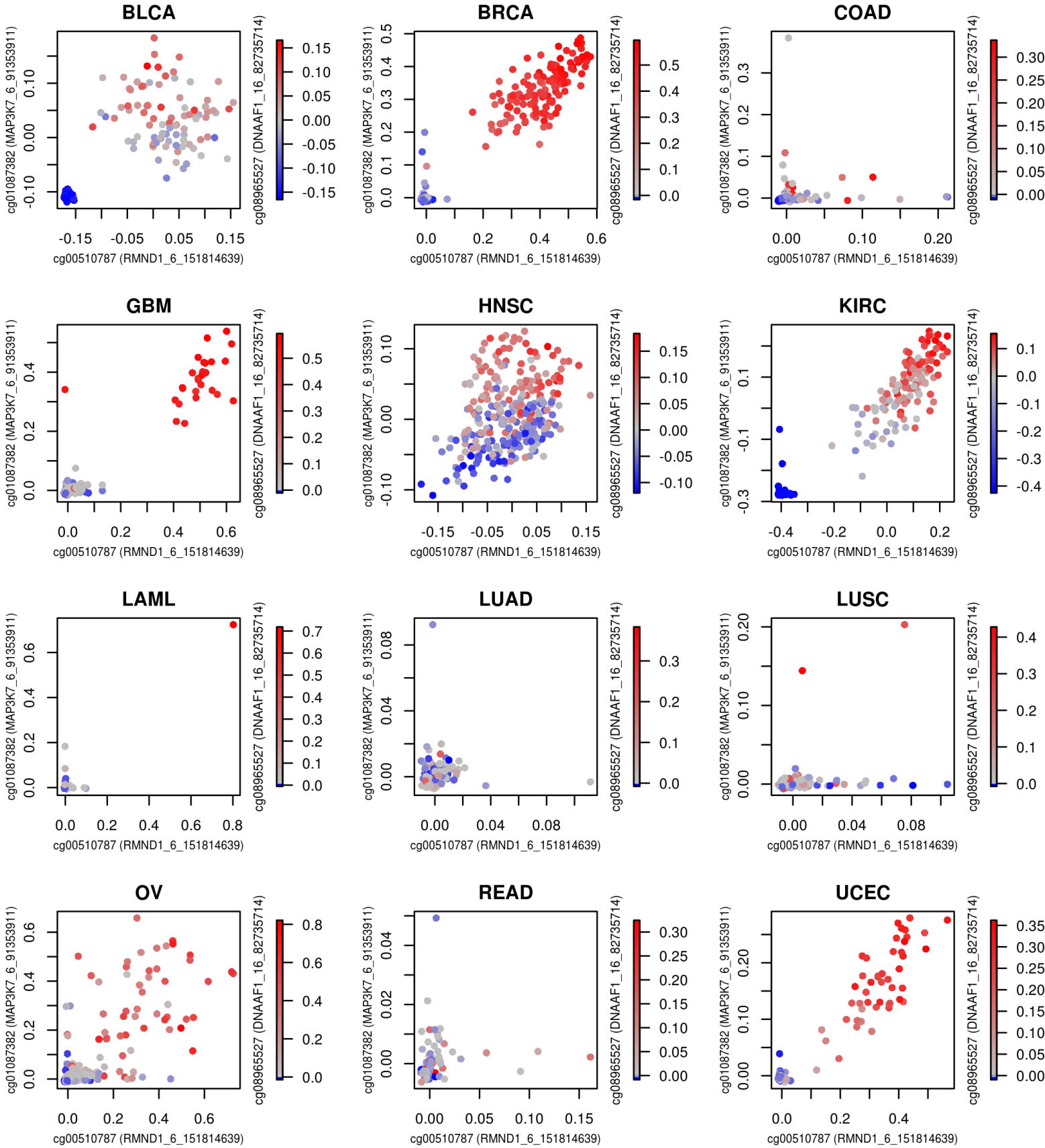
12. mir509 miRNA attractor



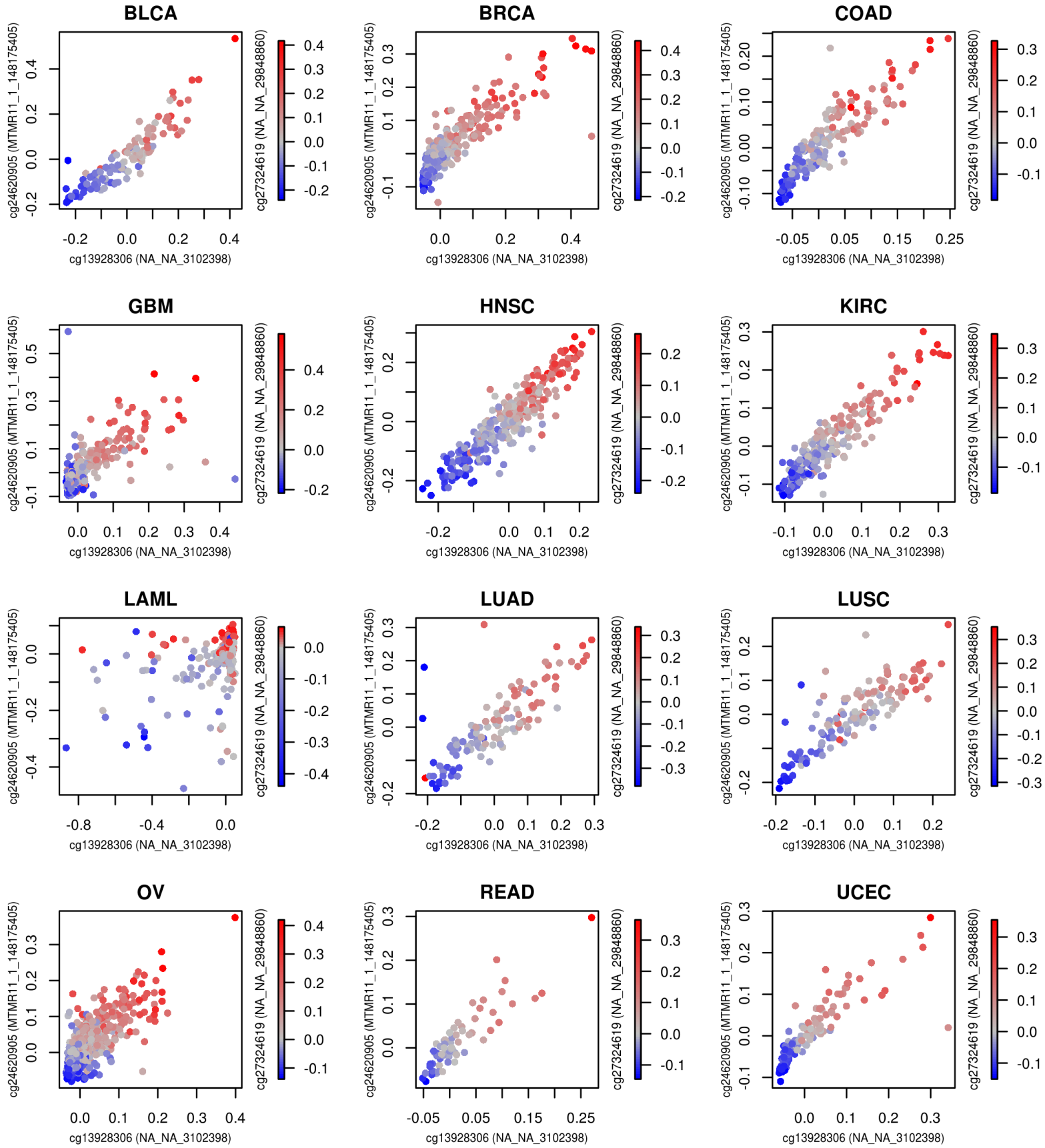
13. mir509 miRNA attractor



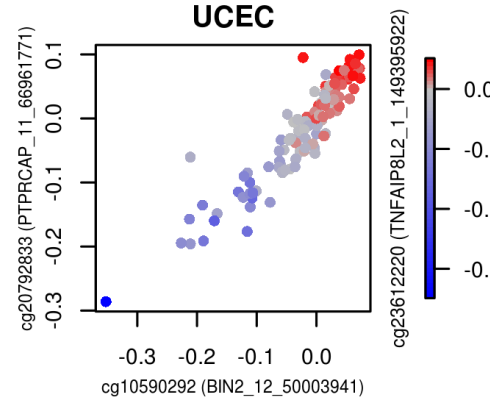
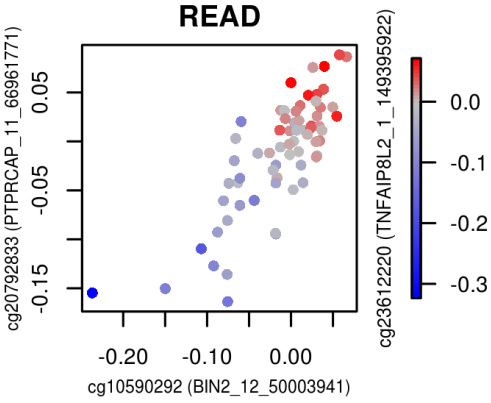
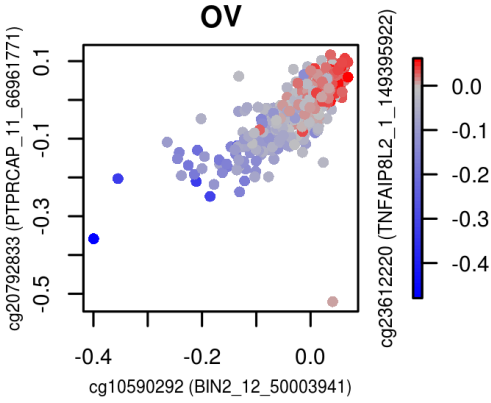
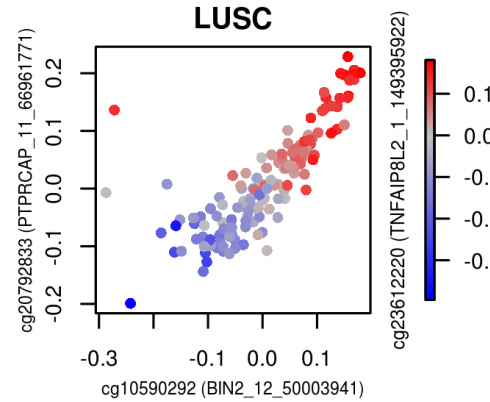
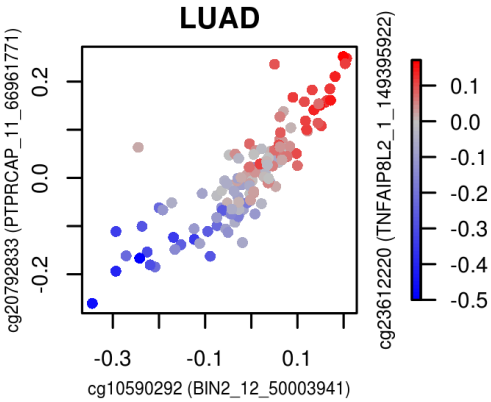
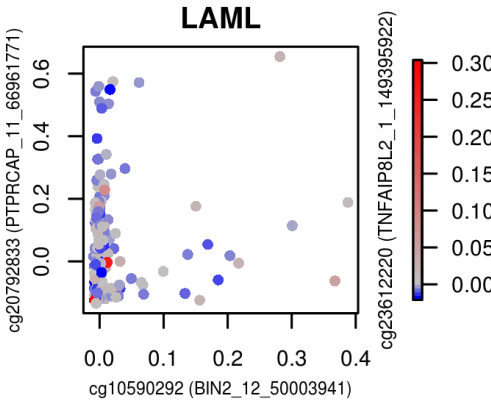
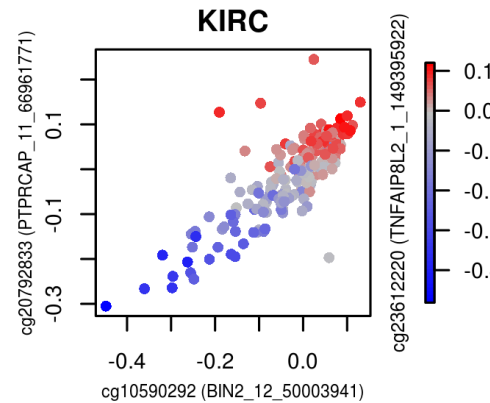
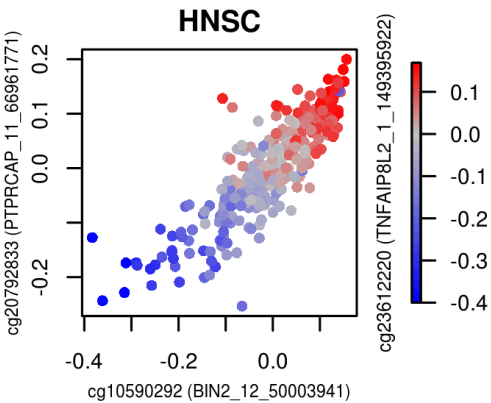
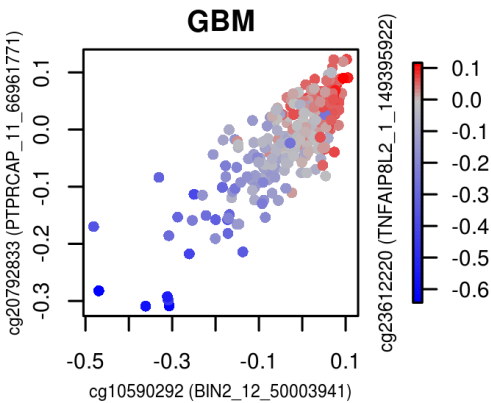
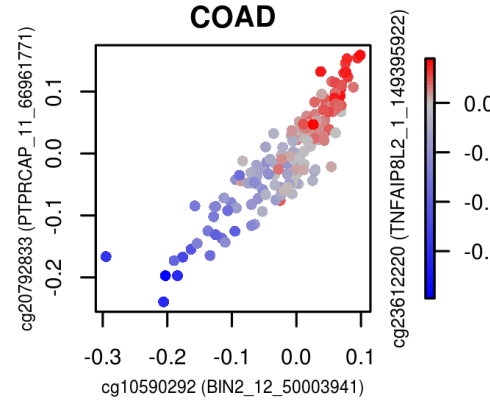
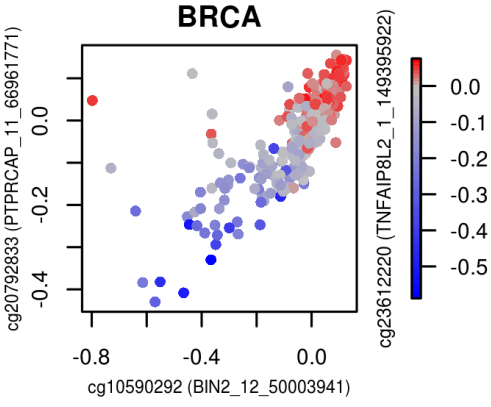
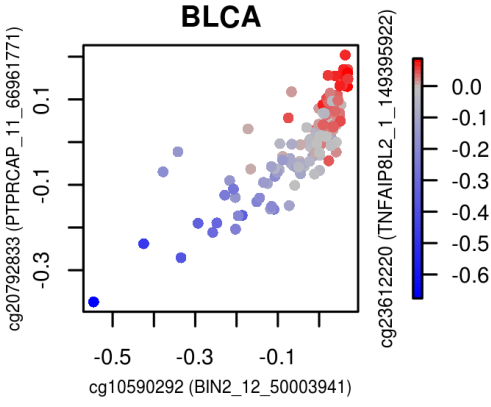
14. RMND1 methylation attractor



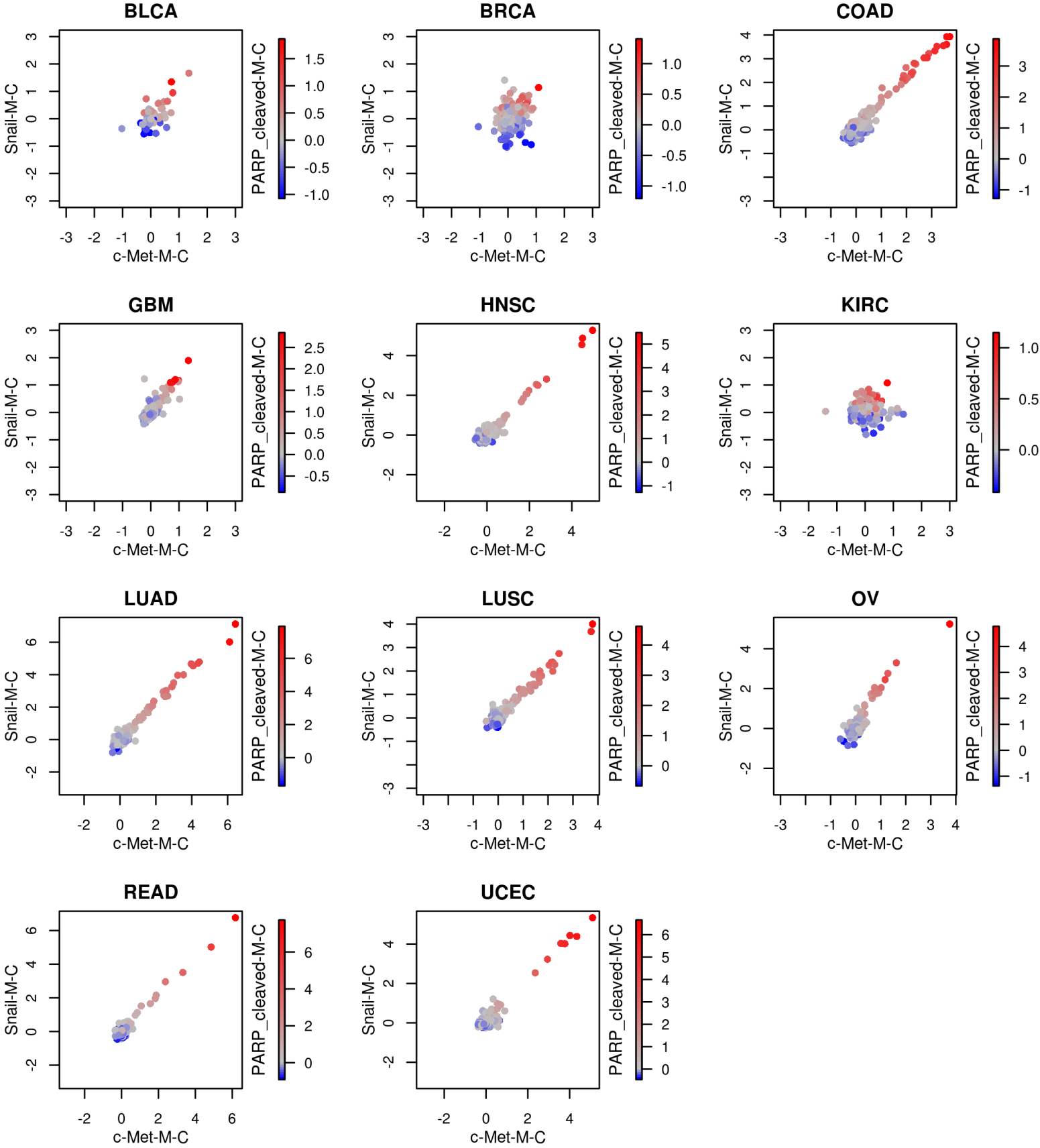
15. M+ methylation attractor



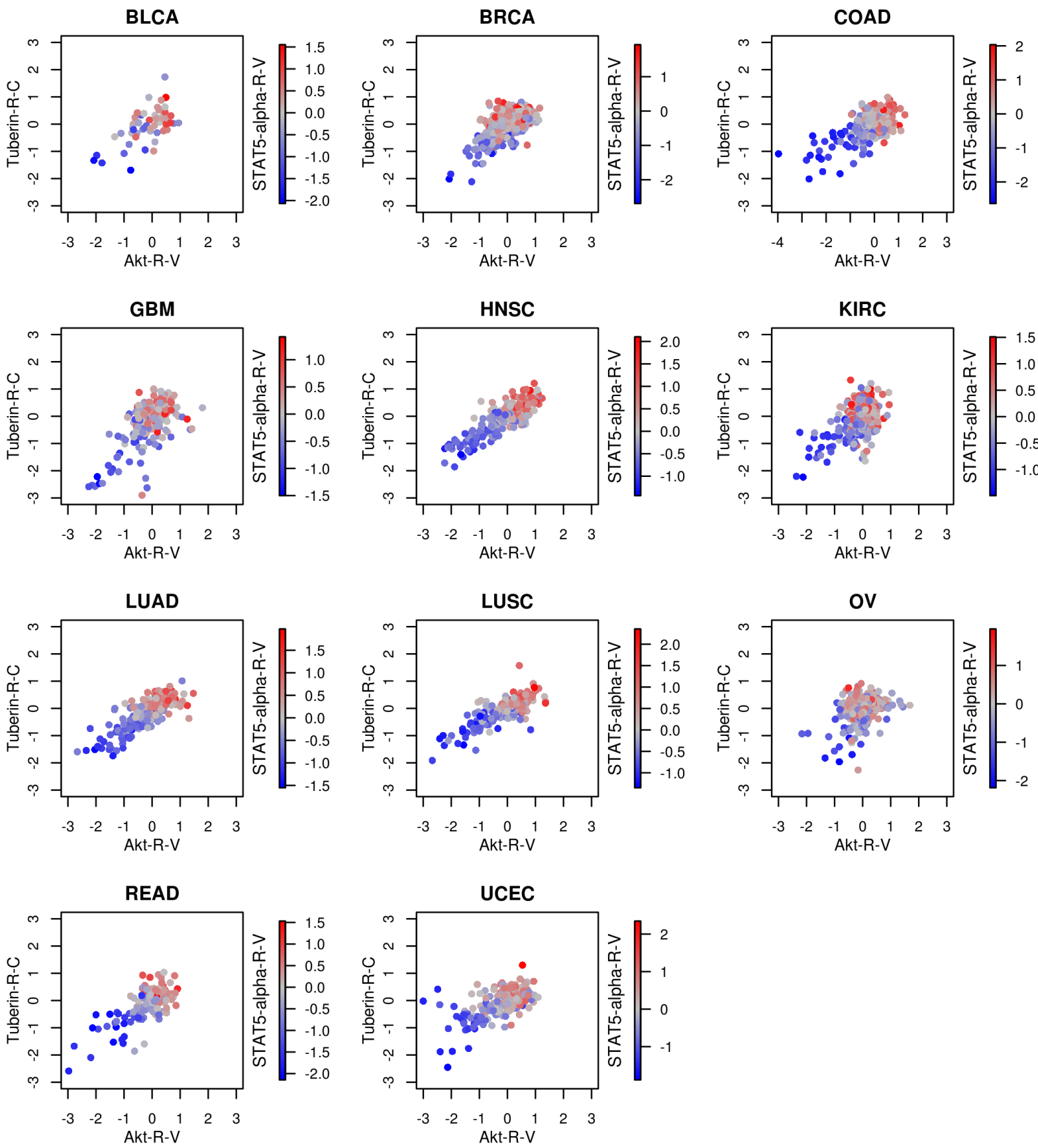
16. M- methylation attractor



17. c-Met protein attractor



18. Akt protein attractor



Supplementary Tables

Table S1: The consensus rankings of features in each attractor.

Rank	Gene Symbol—Entrez ID	Score	Rank	Gene Symbol—Entrez ID	Score
LYM mRNA attractor					
1	SASH3—54440	0.848	85	P2RY10—27334	0.582
2	CD53—963	0.837	86	CD300LF—146722	0.58
3	NCKAP1L—3071	0.783	87	HLA-DRA—3122	0.578
4	LCP2—3937	0.781	88	NCF1—653361	0.576
5	IL10RA—3587	0.78	89	LILRB4—11006	0.575
6	PTPRC—5788	0.774	90	FCGR1A—2209	0.573
7	EVI2B—2124	0.765	91	P2RY13—53829	0.571
8	BIN2—51411	0.752	92	SLC7A7—9056	0.571
9	WAS—7454	0.738	93	C1orf162—128346	0.571
10	HAVCR2—84868	0.735	94	C17orf87—388325	0.567
11	MYO1F—4542	0.735	95	CXorf21—80231	0.567
12	CCR5—1234	0.735	96	CYTIP—9595	0.567
13	SPI1—6688	0.729	97	NFAM1—150372	0.566
14	SELPLG—6404	0.728	98	CORO1A—11151	0.566
15	CYTH4—27128	0.724	99	GIMAP6—474344	0.566
16	SLA—6503	0.723	100	LST1—7940	0.566
17	LAIR1—3903	0.72	101	ARHGAP30—257106	0.564
18	LAPTM5—7805	0.719	102	RCSD1—92241	0.563
19	PLEK—5341	0.712	103	IL2RG—3561	0.562
20	BTK—695	0.707	104	PTPN7—5778	0.556
21	FERMT3—83706	0.702	105	FPR3—2359	0.555
22	CYBB—1536	0.699	106	CD14—929	0.553
23	ITGAL—3683	0.698	107	FYB—2533	0.552
24	CD4—920	0.693	108	GIMAP1—170575	0.552
25	ARHGAP9—64333	0.691	109	IL2RB—3560	0.551
26	LILRB1—10859	0.688	110	SH2D1A—4068	0.551
27	SLAMF8—56833	0.685	111	TNFSF13B—10673	0.55
28	MPEG1—219972	0.683	112	TRAF3IP3—80342	0.549
29	C1QA—712	0.681	113	CMKLR1—1240	0.546
30	CD37—951	0.679	114	CXCR6—10663	0.545
31	ABI3—51225	0.679	115	CCR2—729230	0.545
32	MS4A6A—64231	0.678	116	GIMAP7—168537	0.544
33	ITGB2—3689	0.674	117	GMFG—9535	0.544
34	FCER1G—2207	0.674	118	SRGN—5552	0.542
35	DOK2—9046	0.672	119	CCR1—1230	0.542
36	SNX20—124460	0.672	120	LYZ—4069	0.541
37	C1QB—713	0.668	121	TLR7—51284	0.541
38	GIMAP4—55303	0.667	122	IFI30—10437	0.54
39	CD2—914	0.665	123	SLAMF1—6504	0.538

Continued on next page...

TableS1 – continued from previous page

Rank	Gene Symbol—Entrez ID	Score	Rank	Gene Symbol—Entrez ID	Score
40	AIF1—199	0.665	124	FCGR1B—2210	0.537
41	IL21R—50615	0.656	125	LPXN—9404	0.536
42	TYROBP—7305	0.656	126	PTPN22—26191	0.535
43	CD48—962	0.652	127	LY86—9450	0.534
44	APBB1IP—54518	0.65	128	HLA-DMB—3109	0.534
45	C1QC—714	0.649	129	KIAA0748—9840	0.533
46	CD3E—916	0.644	130	IL16—3603	0.532
47	GIMAP5—55340	0.641	131	CSF2RB—1439	0.532
48	RASAL3—64926	0.64	132	CD3D—915	0.532
49	SPN—6693	0.637	133	WIPF1—7456	0.531
50	C3AR1—719	0.635	134	SIGLEC7—27036	0.53
51	GPR65—8477	0.631	135	DOK3—79930	0.529
52	FGL2—10875	0.629	136	SIRPG—55423	0.527
53	TAGAP—117289	0.629	137	TIGIT—201633	0.525
54	MNDA—4332	0.628	138	RHOH—399	0.524
55	EVI2A—2123	0.627	139	ACAP1—9744	0.524
56	CSF1R—1436	0.625	140	CD247—919	0.523
57	DOCK2—1794	0.623	141	SLA2—84174	0.522
58	IRF8—3394	0.621	142	UBASH3A—53347	0.522
59	SIGLEC10—89790	0.621	143	NCF4—4689	0.52
60	SAMSN1—64092	0.619	144	GAB3—139716	0.52
61	IKZF1—10320	0.618	145	CD52—1043	0.519
62	HLA-DPB1—3115	0.617	146	CTSS—1520	0.518
63	CD86—942	0.615	147	ITGAX—3687	0.516
64	SLAMF6—114836	0.614	148	CCL5—6352	0.514
65	TFEC—22797	0.611	149	SIT1—27240	0.514
66	CD84—8832	0.611	150	PARVG—64098	0.514
67	IGSF6—10261	0.608	151	PYHIN1—149628	0.513
68	SLCO2B1—11309	0.608	152	NKG7—4818	0.512
69	LILRB2—10288	0.608	153	CD300A—11314	0.512
70	HLA-DPA1—3113	0.606	154	LOC100233209—100233209	0.512
71	LAT2—7462	0.603	155	GZMK—3003	0.511
72	TNFAIP8L2—79626	0.601	156	AOAH—313	0.509
73	ARHGAP15—55843	0.596	157	CD180—4064	0.509
74	FAM78A—286336	0.594	158	MS4A7—58475	0.508
75	TLR8—51311	0.593	159	GVIN1—387751	0.508
76	ITK—3702	0.593	160	CD33—945	0.507
77	FCGR3A—2214	0.592	161	FGD2—221472	0.506
78	HCST—10870	0.591	162	LY9—4063	0.505
79	IL12RB1—3594	0.59	163	MS4A4A—51338	0.505
80	LRRC25—126364	0.588	164	FMNL1—752	0.503
81	PIK3R5—23533	0.584	165	FGR—2268	0.502

Continued on next page...

TableS1 – continued from previous page

Rank	Gene Symbol—Entrez ID	Score	Rank	Gene Symbol—Entrez ID	Score
82	CXCR3—2833	0.584	166	TRPV2—51393	0.502
83	RNASE6—6039	0.583	167	HCK—3055	0.501
84	TNFRSF1B—7133	0.582	168	WDFY4—57705	0.501
CIN mRNA attractor					
1	TPX2—22974	0.776	48	SKA1—220134	0.604
2	KIF4A—24137	0.753	49	CENPF—1063	0.602
3	KIFC1—3833	0.734	50	NDC80—10403	0.598
4	NCAPG—64151	0.732	51	CEP55—55165	0.597
5	BUB1—699	0.73	52	CDC6—990	0.597
6	NCAPH—23397	0.729	53	BIRC5—332	0.596
7	CDCA5—113130	0.725	54	CDK1—983	0.59
8	KIF2C—11004	0.725	55	ARHGAP11A—9824	0.584
9	PLK1—5347	0.723	56	RAD54L—8438	0.583
10	CENPA—1058	0.709	57	STIL—6491	0.583
11	TOP2A—7153	0.702	58	CDC45—8318	0.581
12	HJURP—55355	0.702	59	DTL—51514	0.581
13	BUB1B—701	0.698	60	CDC25C—995	0.579
14	KIF23—9493	0.691	61	DEPDC1B—55789	0.569
15	FOXM1—2305	0.69	62	EPR1—8475	0.561
16	MCM10—55388	0.687	63	CCNB1—891	0.556
17	KIF18B—146909	0.683	64	ERCC6L—54821	0.55
18	CCNA2—890	0.677	65	MKI67—4288	0.55
19	GTSE1—51512	0.676	66	KIF18A—81930	0.548
20	CKAP2L—150468	0.676	67	SPC25—57405	0.546
21	CCNB2—9133	0.676	68	GSG2—83903	0.543
22	DLGAP5—9787	0.674	69	CDCA3—83461	0.543
23	KIF11—3832	0.672	70	CENPI—2491	0.541
24	CDCA8—55143	0.666	71	CENPE—1062	0.54
25	KIF14—9928	0.663	72	CDCA2—157313	0.537
26	MELK—9833	0.662	73	FANCI—55215	0.537
27	NEK2—4751	0.651	74	POLQ—10721	0.535
28	AURKB—9212	0.649	75	RAD51—5888	0.53
29	PRC1—9055	0.646	76	C15orf42—90381	0.526
30	ASPM—259266	0.644	77	KPNA2—3838	0.521
31	KIF20A—10112	0.643	78	ZWINT—11130	0.521
32	EXO1—9156	0.642	79	FAM72B—653820	0.519
33	CDC20—991	0.642	80	ESCO2—157570	0.516
34	MYBL2—4605	0.64	81	PLK4—10733	0.515
35	RACGAP1—29127	0.633	82	ASF1B—55723	0.514
36	RRM2—6241	0.632	83	ECT2—1894	0.513
37	SGOL1—151648	0.631	84	ESPL1—9700	0.513
38	DEPDC1—55635	0.629	85	LMNB1—4001	0.511

Continued on next page...

TableS1 – continued from previous page

Rank	Gene Symbol—Entrez ID	Score	Rank	Gene Symbol—Entrez ID	Score
39	ORC1L—4998	0.627	86	SPAG5—10615	0.51
40	TROAP—10024	0.625	87	FAM64A—54478	0.51
41	UBE2C—11065	0.62	88	PTTG1—9232	0.508
42	TTK—7272	0.62	89	CASC5—57082	0.506
43	SKA3—221150	0.614	90	CDKN3—1033	0.505
44	AURKA—6790	0.613	91	UHRF1—29128	0.504
45	KIF15—56992	0.612	92	SHCBP1—79801	0.504
46	NUSAP1—51203	0.609	93	OIP5—11339	0.501
47	NUF2—83540	0.608	94	PBK—55872	0.501
MES mRNA attractor					
1	COL3A1—1281	0.798	31	SFRP2—6423	0.572
2	COL5A2—1290	0.775	32	FNDC1—84624	0.567
3	COL1A2—1278	0.771	33	ISLR—3671	0.559
4	THBS2—7058	0.753	34	COL10A1—1300	0.554
5	COL5A1—1289	0.746	35	CRISPLD2—83716	0.551
6	VCAN—1462	0.726	36	COL8A1—1295	0.549
7	COL6A3—1293	0.717	37	BNC2—54796	0.545
8	SPARC—6678	0.715	38	LUM—4060	0.543
9	AEBP1—165	0.709	39	ANTXR1—84168	0.542
10	FBN1—2200	0.705	40	THY1—7070	0.539
11	POSTN—10631	0.683	41	ASPN—54829	0.537
12	FAP—2191	0.654	42	COL6A1—1291	0.537
13	MMP2—4313	0.646	43	NID2—22795	0.533
14	COL1A1—1277	0.644	44	COL11A1—1301	0.531
15	PDGFRB—5159	0.641	45	DACT1—51339	0.53
16	LRRC15—131578	0.64	46	FN1—2335	0.53
17	ADAMTS2—9509	0.631	47	LAMA4—3910	0.528
18	ITGA11—22801	0.63	48	SULF1—23213	0.526
19	ADAM12—8038	0.628	49	GPR124—25960	0.524
20	OLFML2B—25903	0.622	50	CCDC80—151887	0.524
21	EMILIN1—11117	0.607	51	MXRA5—25878	0.523
22	COL6A2—1292	0.607	52	OLFML1—283298	0.523
23	TIMP2—7077	0.592	53	CTHRC1—115908	0.52
24	CDH11—1009	0.591	54	PCOLCE—5118	0.516
25	GLT8D2—83468	0.591	55	ACTA2—59	0.51
26	CTSK—1513	0.588	56	GREM1—26585	0.509
27	PRRX1—5396	0.587	57	DCN—1634	0.508
28	ADAMTS12—81792	0.585	58	CALD1—800	0.503
29	ANGPTL2—23452	0.584	59	MSRB3—253827	0.501
30	BGN—633	0.574			
END mRNA attractor					
1	CDH5—1003	0.813	15	RHOJ—57381	0.6

Continued on next page...

TableS1 – continued from previous page

Rank	Gene Symbol—Entrez ID	Score	Rank	Gene Symbol—Entrez ID	Score
2	ROBO4—54538	0.771	16	BCL6B—255877	0.573
3	CXorf36—79742	0.761	17	TEK—7010	0.567
4	CD34—947	0.733	18	GPR116—221395	0.563
5	CLEC14A—161198	0.688	19	ACVRL1—94	0.56
6	ARHGEF15—22899	0.673	20	ECSCR—641700	0.551
7	CD93—22918	0.672	21	VWF—7450	0.549
8	LDB2—9079	0.67	22	KDR—3791	0.547
9	ELTD1—64123	0.667	23	EMCN—51705	0.533
10	MYCT1—80177	0.661	24	PTPRB—5787	0.517
11	TIE1—7075	0.661	25	NOTCH4—4855	0.515
12	S1PR1—1901	0.653	26	ERG—2078	0.514
13	ESAM—90952	0.64	27	PECAM1—5175	0.507
14	PCDH12—51294	0.605			
AHSA2 mRNA attractor					
1	AHSA2—130872	0.775	15	CSAD—51380	0.545
2	LOC91316—91316	0.641	16	GOLGA8B—440270	0.539
3	PILRB—29990	0.63	17	GOLGA8A—23015	0.535
4	ZNF767—79970	0.63	18	NCRNA00105—80161	0.522
5	TTL3—26140	0.612	19	CROCCL2—114819	0.521
6	CCNL2—81669	0.606	20	?—155060	0.52
7	PABPC1L—80336	0.606	21	AGAP4—119016	0.52
8	LENG8—114823	0.602	22	LOC100272228—100272228	0.517
9	CHKB-CPT1B—386593	0.595	23	LUC7L3—51747	0.517
10	SEC31B—25956	0.585	24	C1orf104—284618	0.512
11	NKTR—4820	0.57	25	NCRNA00201—284702	0.51
12	AGAP6—414189	0.569	26	WASH7P—653635	0.504
13	PDXDC2—283970	0.545	27	LOC100131434—100131434	0.504
14	HERC2P2—400322	0.545			
IFIT mRNA attractor					
1	IFIT3—3437	0.779	11	IFIT2—3433	0.594
2	MX1—4599	0.761	12	XAF1—54739	0.59
3	OAS2—4939	0.757	13	OASL—8638	0.589
4	RSAD2—91543	0.753	14	ISG15—9636	0.565
5	CMPK2—129607	0.741	15	HERC6—55008	0.56
6	IFIT1—3434	0.732	16	OAS3—4940	0.552
7	IFI44L—10964	0.721	17	IFIH1—64135	0.552
8	IFI44—10561	0.695	18	DDX58—23586	0.54
9	IFI6—2537	0.644	19	DDX60—55601	0.512
10	OAS1—4938	0.613			
WDR38 mRNA attractor					
1	WDR38—401551	0.677	11	C9orf171—389799	0.563
2	YSK4—80122	0.623	12	CCDC135—84229	0.559

Continued on next page...

TableS1 – continued from previous page

Rank	Gene Symbol—Entrez ID	Score	Rank	Gene Symbol—Entrez ID	Score
3	ROPN1L—83853	0.613	13	C1orf192—257177	0.557
4	C1orf194—127003	0.603	14	CAPSL—133690	0.554
5	MORN5—254956	0.597	15	ZBBX—79740	0.553
6	WDR16—146845	0.587	16	CCDC42B—387885	0.523
7	RSPH4A—345895	0.577	17	C1orf92—149499	0.522
8	FAM183A—440585	0.574	18	C2orf39—92749	0.511
9	ZMYND10—51364	0.565	19	DNAH12—201625	0.508
10	DNAI1—27019	0.564	20	RSPH1—89765	0.505
MHC Class II GL mRNA attractor – chr6p21.32					
1	HLA-DPA1—3113	0.865	6	HLA-DMB—3109	0.734
2	HLA-DRA—3122	0.859	7	HLA-DOA—3111	0.674
3	HLA-DPB1—3115	0.787	8	HLA-DQA1—3117	0.614
4	HLA-DRB1—3123	0.76	9	HLA-DRB5—3127	0.503
5	HLA-DMA—3108	0.746	10	HLA-DQB1—3119	0.387
GIMAP GL mRNA attractor – chr7q36.1					
1	GIMAP4—55303	0.553	6	GIMAP1—170575	0.471
2	GIMAP7—168537	0.55	7	GIMAP2—26157	0.269
3	GIMAP6—474344	0.547	8	TMEM176B—28959	0.179
4	GIMAP5—55340	0.539	9	TMEM176A—55365	0.143
5	GIMAP8—155038	0.495	10	ZNF777—27153	0.127
chr8q24.3 GL mRNA attractor					
1	SHARPIN—81858	0.585	6	EXOSC4—54512	0.339
2	HSF1—3297	0.575	7	SCRIB—23513	0.307
3	TIGD5—84948	0.535	8	CYHR1—50626	0.294
4	GPR172A—79581	0.482	9	MAF1—84232	0.246
5	ZC3H3—23144	0.42	10	PUF60—22827	0.234

Rank	Probe	GeneSymbol-Chr-Location	Score	Rank	Probe	GeneSymbol-Chr-Location	Score
RMND1 methylation attractor							
1	cg00510787	RMND1-6-151814639	0.842	61	cg18325289	USP48-1-21982534	0.586
2	cg01087382	MAP3K7-6-91353911	0.836	62	cg17607973	MEPCE-7-99865344	0.586
3	cg08965527	DNAAF1-16-82735714	0.822	63	cg11628034	RPS16-19-44618744	0.579
4	cg08793459	PTRH2-17-55139429	0.819	64	cg25409040	CSTF3-11-33139919	0.579
5	cg14037413	ZNF143-11-9439170	0.817	65	cg09747578	LRRC41-1-46541663	0.576
6	cg03627896	NA-NA-30841835	0.805	66	cg16016641	C2orf4-20-34287611	0.574
7	cg03169527	TAMM41-3-11863582	0.804	67	cg26979012	PSMC6-14-52243814	0.574
8	cg11368578	CDK5-7-150385869	0.787	68	cg24356797	UBA52-19-18543387	0.573
9	cg19233923	OTUB1-11-63510174	0.781	69	cg26258330	ZFAND1-8-82795685	0.572
10	cg25742201	AATF-17-32380976	0.78	70	cg22468803	ANKRD12-18-9126381	0.571
11	cg20684973	TAF5-10-105117622	0.779	71	cg01439983	PEX13-2-61097497	0.567
12	cg06719391	NA-NA-2510906	0.776	72	cg02776251	USP15-12-60940586	0.565

Continued on next page...

TableS1 – continued from previous page

Rank	Probe	GeneSymbol-Chr-Location	Score	Rank	Probe	GeneSymbol-Chr-Location	Score
13	cg23179321	RPP38-10-15178799	0.775	73	cg19469297	TBRG4-7-45117965	0.562
14	cg25346576	NSRP1-17-25467978	0.756	74	cg26477793	ACTR1A-10-104252075	0.561
15	cg04305134	ANXA7-10-74843380	0.743	75	cg27196102	COG7-16-23372214	0.56
16	cg24568646	CCT8-21-29368109	0.739	76	cg01998146	PSIP1-9-15501358	0.558
17	cg23347958	DHX8-17-38916826	0.731	77	cg24695828	ZNF566-19-41672097	0.557
18	cg08209724	ZNF207-17-27701251	0.729	78	cg12790134	VCPIP1-8-67741341	0.553
19	cg15749322	ANKRD42-11-82582847	0.728	79	cg16141690	C14orf119-14-22633555	0.551
20	cg26538116	LRPPRC-2-44076832	0.726	80	cg01466020	YY1AP1-1-153925818	0.55
21	cg26446827	ZNF133-20-18216978	0.726	81	cg15875120	FAM188A-10-15942611	0.547
22	cg09047884	TTL1-22-41814928	0.725	82	cg11084020	TAX1BP1-7-27746092	0.544
23	cg25418748	RUFY1-5-178909842	0.724	83	cg27546682	STK40-1-36624447	0.544
24	cg24654547	DUS2L-16-66614666	0.72	84	cg15009698	AP3B1-5-77626250	0.542
25	cg12662162	C6orf106-6-34772865	0.711	85	cg03100196	ZYX-7-142787883	0.542
26	cg17718515	IPO9-1-200065440	0.698	86	cg19747852	TRA2A-7-23538218	0.541
27	cg21605986	KIAA1191-5-175721331	0.691	87	cg13022174	SS18-18-21925057	0.54
28	cg06611744	RASL11A-13-26742618	0.688	88	cg17159242	RPS7-2-3600935	0.539
29	cg08871016	HSF2BP-21-43903660	0.682	89	cg05856931	MSI2-17-52688096	0.536
30	cg11011602	RPL7A-9-135204850	0.68	90	cg08529259	GCSH-16-79686870	0.536
31	cg07979357	IL27RA-19-14003353	0.68	91	cg16769442	MAGI3-1-113735582	0.536
32	cg25658980	PIH1D1-19-54646816	0.679	92	cg24478630	MOGS-2-74546204	0.535
33	cg05577173	PAPD4-5-78944434	0.675	93	cg16425577	DENND3-8-142208836	0.532
34	cg03843852	PIGB-15-53398391	0.672	94	cg07209631	PPM1K-4-89424752	0.532
35	cg23213688	EXOC8-1-229540414	0.667	95	cg27227786	DGKE-17-52266264	0.53
36	cg21643860	TUT1-11-62115390	0.663	96	cg08158331	SH2D6-2-85499059	0.53
37	cg16854524	LIN54-4-84150926	0.658	97	cg18142353	LRP6-12-12311841	0.528
38	cg20188282	GTF3C5-9-134896021	0.656	98	cg08613513	ORC1-1-52642648	0.527
39	cg21589280	DDAH1-1-85702739	0.654	99	cg12835684	MFSD5-12-51931914	0.526
40	cg20908993	ATP6V1D-14-66896131	0.65	100	cg08717396	HIST1H2AG-6-27208754	0.524
41	cg14191109	SLC25A16-10-69957444	0.649	101	cg19857457	RPL17-18-45272945	0.522
42	cg27072323	CAP1-1-40279445	0.647	102	cg17868994	NIPSNAP3B-9-106566104	0.521
43	cg21666675	CHCHD4-3-14140844	0.646	103	cg15806518	PSMB7-9-126217638	0.521
44	cg08358671	IVNS1ABP-1-183553430	0.64	104	cg03863549	NOL6-9-33464004	0.521
45	cg23749163	KIAA1737-14-76633721	0.639	105	cg01449415	ZNF213-16-3124812	0.52
46	cg21452766	CTH-1-70649676	0.636	106	cg11371394	TGFBRAP1-2-105313015	0.519
47	cg03532005	PSPH-7-56086522	0.635	107	cg08554462	NA-NA-59137891	0.519
48	cg07031532	OAZ2-15-62782737	0.632	108	cg09378940	LACTB2-8-71743860	0.518
49	cg09507928	IK-5-140007668	0.63	109	cg25264554	XRN1-3-143649479	0.518
50	cg05797656	DDX42-17-59205084	0.629	110	cg10095719	NRP1-10-33663793	0.517
51	cg23526055	TCEB1-8-75047348	0.627	111	cg22721186	ATAD2-8-124478099	0.517
52	cg08376864	HRASLS-3-194441420	0.622	112	cg16268429	NADKD1-5-36277893	0.516
53	cg06422693	OCIAD1-4-48528344	0.618	113	cg21546057	FIBP-11-65412902	0.516
54	cg20760063	NA-NA-38531106	0.616	114	cg21824902	WDTC1-1-27433419	0.512

Continued on next page...

TableS1 – continued from previous page

Rank	Probe	GeneSymbol-Chr-Location	Score	Rank	Probe	GeneSymbol-Chr-Location	Score
55	cg14817848	DUSP16-12-12606825	0.615	115	cg22176017	POLR2G-11-62286036	0.511
56	cg23653187	PNPLA3-22-42650590	0.603	116	cg14711201	SKP2-5-36188193	0.511
57	cg04883450	DIMT1-5-61735714	0.601	117	cg07820214	RUVBL1-3-129325679	0.511
58	cg22464182	ACVR2A-2-148319095	0.595	118	cg15452426	DFFA-1-10454817	0.507
59	cg21097640	POLR1D-13-27093548	0.593	119	cg16050957	RBBP6-16-24458244	0.506
60	cg01190915	MT2A-16-55200262	0.587	120	cg00115714	AMD1-6-111302805	0.503
M+ methylation attractor							
1	cg13928306	NA-NA-3102398	0.72	41	cg27238470	EDN2-1-41722912	0.566
2	cg24620905	MTMR11-1-148175405	0.719	42	cg03684977	GRB7-17-35147329	0.565
3	cg27324619	NA-NA-29848860	0.713	43	cg09243900	RAB25-1-154297468	0.562
4	cg12603560	TNKS1BP1-11-56846646	0.712	44	cg26531804	SPINT1-15-38923139	0.559
5	cg08775230	C11orf52-11-111294703	0.709	45	cg08463485	ILDR1-3-123223617	0.556
6	cg07705835	IL17RC-3-9934128	0.703	46	cg10917602	HSD3B7-16-30904131	0.553
7	cg24765079	NA-NA-67329931	0.694	47	cg22585988	PVRL4-1-159325951	0.552
8	cg19258882	ERBB3-12-54759072	0.683	48	cg01919208	LAMB2-3-49145500	0.551
9	cg09152089	IL22RA1-1-24342151	0.68	49	cg10212621	HMGCS2-1-120113172	0.551
10	cg05697249	C11orf52-11-111294903	0.677	50	cg17186163	C10orf10-10-44794323	0.548
11	cg18053607	NA-NA-29848963	0.663	51	cg18988110	PRR15L-17-43390342	0.547
12	cg14036856	C1orf210-1-43524150	0.65	52	cg23349242	SUSD2-22-22907448	0.545
13	cg04245402	C19orf21-19-702241	0.649	53	cg05225996	NA-NA-3103018	0.544
14	cg20324165	KRT8-12-51585412	0.638	54	cg13530039	CHRM1-11-62446133	0.542
15	cg13439730	PRSS8-16-31054500	0.63	55	cg20484352	FAM114A1-4-38546174	0.537
16	cg24433189	SSTR5-16-1068690	0.622	56	cg09440340	MAB21L3-1-116455938	0.535
17	cg16176600	FRK-6-116488302	0.617	57	cg22764925	GGT1-22-23309964	0.533
18	cg25370441	ARHGEF38-4-106692682	0.612	58	cg14528319	GIPC1-19-14468713	0.532
19	cg09307264	INCA1-17-4843005	0.61	59	cg07947930	PRELP-1-201711568	0.532
20	cg17826679	SLC44A2-19-10597038	0.609	60	cg22780475	CBLC-19-49973366	0.53
21	cg00698688	SULT2B1-19-53747244	0.603	61	cg05245515	SLC39A2-14-20537113	0.526
22	cg09548084	SLC35B3-6-8381217	0.602	62	cg17740645	GRB7-17-35147939	0.524
23	cg21663431	SLC44A2-19-10597355	0.601	63	cg18565355	ESRP1-8-95723050	0.523
24	cg25946374	IL22RA1-1-24342378	0.599	64	cg25415932	OGG1-3-9766051	0.521
25	cg22580512	NCOR2-12-123568427	0.59	65	cg02537838	C20orf151-20-60435990	0.52
26	cg16986846	SCGB2A1-11-61732750	0.59	66	cg19923326	NA-NA-2785354	0.519
27	cg05517572	STAP2-19-4289769	0.588	67	cg23165541	DAPK2-15-62125217	0.517
28	cg16787352	ANKRD9-14-102045158	0.587	68	cg03599338	SUSD2-22-22907315	0.516
29	cg24210717	GPD1-12-48784094	0.584	69	cg01835489	KRT8-12-51585577	0.513
30	cg27126442	ARHGEF38-4-106693255	0.583	70	cg03003745	CXCL17-19-47640007	0.513
31	cg19759064	PHKG1-7-56128181	0.579	71	cg00451635	EMP2-16-10582531	0.512
32	cg05228408	CLCN6-1-11787939	0.579	72	cg23323671	STMN1-1-26106210	0.508
33	cg14322224	DDAH1-1-85703814	0.578	73	cg04806409	TFF3-21-42608574	0.508
34	cg12894126	UCK1-9-133395746	0.577	74	cg03109701	RNFT2-12-115659141	0.508
35	cg09871043	PKHD1-6-52060320	0.575	75	cg22820108	NCOR2-12-123569171	0.508

Continued on next page...

TableS1 – continued from previous page

Rank	Probe	GeneSymbol-Chr-Location	Score	Rank	Probe	GeneSymbol-Chr-Location	Score
36	cg02293044	GAS2L1-22-28033543	0.574	76	cg08445039	FKBP9-7-32964184	0.507
37	cg02237119	WBSCR27-7-72894350	0.574	77	cg18632631	TNK1-17-7224773	0.504
38	cg00480115	FXYD3-19-40298717	0.57	78	cg01119135	C1orf116-1-205272148	0.503
39	cg24751129	GNMT-6-43036898	0.569	79	cg21201572	AGR2-7-16811131	0.501
40	cg04001668	GPR56-16-56211848	0.566	80	cg24835159	RNF43-17-53849553	0.501
M- methylation attractor							
1	cg10590292	BIN2-12-50003941	0.72	15	cg15352829	PLD4-14-104462063	0.576
2	cg20792833	PTPRCAP-11-66961771	0.659	16	cg07380416	CD6-11-60495748	0.576
3	cg23612220	TNFAIP8L2-1-149395922	0.653	17	cg23953831	CD101-1-117345939	0.567
4	cg16927606	IGFLR1-19-40925164	0.64	18	cg03569637	FAM113B-12-45895624	0.559
5	cg05596756	FAM113B-12-45896487	0.635	19	cg14145194	ICAM3-19-10311022	0.557
6	cg09902130	CD6-11-60495754	0.61	20	cg26683005	CARD8-19-53444802	0.553
7	cg20425130	KLHL6-3-184755939	0.602	21	cg07732037	MPHOSPH9-12-122273780	0.55
8	cg18384097	PTPN7-1-200396189	0.601	22	cg11600161	TBC1D10C-11-66928161	0.535
9	cg17936488	FAM78A-9-133141340	0.601	23	cg01623438	CTSZ-20-57016289	0.529
10	cg25671438	ACAP1-17-7180947	0.598	24	cg23093496	C16orf54-16-29664824	0.523
11	cg16609957	SHROOM1-5-132189766	0.593	25	cg27377213	PPP1R16B-20-36867217	0.519
12	cg14519350	OSM-22-28991949	0.588	26	cg15691199	CEBPE-14-22659259	0.503
13	cg16509569	NCKAP1L-12-53177901	0.582	27	cg15551881	TRAF1-9-122728536	0.503
14	cg07973967	CD79B-17-59363339	0.578				

Rank	miRNA family	Score	Rank	miRNA family	Score
mir-127 miRNA attractor					
1	hsa-mir-127	0.854	9	hsa-mir-654	0.615
2	hsa-mir-134	0.835	10	hsa-mir-431	0.574
3	hsa-mir-379	0.803	11	hsa-mir-493	0.561
4	hsa-mir-409	0.742	12	hsa-mir-337	0.554
5	hsa-mir-382	0.686	13	hsa-mir-487	0.528
6	hsa-mir-758	0.678	14	hsa-mir-889	0.516
7	hsa-mir-381	0.649	15	hsa-mir-154	0.512
8	hsa-mir-370	0.616			
mir-509 miRNA attractor					
1	hsa-mir-509	0.899	3	hsa-mir-508	0.81
2	hsa-mir-514	0.824			
mir-144 miRNA attractor					
1	hsa-mir-144	0.89	3	hsa-mir-486	0.678
2	hsa-mir-451	0.877			

Rank	Protein	Score	Rank	Protein	Score
c-Met protein attractor					

Continued on next page...

TableS1 – continued from previous page

Rank	Protein	Score	Rank	Protein	Score
1	c-Met-M-C	0.877	4	Caspase-8-M-C	0.741
2	Snail-M-C	0.829	5	ERCC1-M-C	0.674
3	PARP_cleaved-M-C	0.763	6	Rb-M-V	0.567
Akt protein attractor					
1	Akt-R-V	0.6	3	STAT5-alpha-R-V	0.519
2	Tuberin-R-C	0.552			